ACS Catalysis

Review

Cite This: ACS Catal. 2019, 9, 10020−10043

pubs.acs.org/acscatalysis

Operando Insights into Nanoparticle Transformations during Catalysis

Arno Bergmann and Beatriz Roldan Cuenya*

Department of Interface Science, Fritz-Haber Institute of the Max Planck Society, Faradayweg 4-6, 14195 Berlin, Germany

ABSTRACT: Nanostructured materials play an important role in today's chemical industry, acting as catalysts in heterogeneous thermal and electrocatalytic processes for chemical energy conversion and the production of feedstock chemicals. Although catalysis research is a longstanding discipline, the fundamental properties of heterogeneous catalysts such as atomic structure, morphology and surface composition under realistic reaction conditions, together with insights into the nature of the catalytically active sites, have remained largely unknown. Having access to such information is however of outmost importance in order to understand the rate-determining processes and steps of many heterogeneous reactions and identify important structure−activity/selectivity relationships, enabling knowledge-driven improvement of catalysts. In the last decades, in situ and operando methods have become available to identify the structural and morphological properties of the catalysts under working conditions. Such investigations have led to important insights into the catalytically active state of the materials at different length scales, from the atomic level to the nano-/micrometer scale. The accessible operando methods utilizing photons range from vibrational spectroscopy in the infrared and optical regime to small-angle X-ray scattering (SAXS), diffraction (XRD), absorption spectroscopy (XAFS), and photoelectron spectroscopy (XPS), whereas electron-based techniques include scanning (SEM) and transmission microscopy (TEM) methods. In this work, we summarize recent findings of structural, morphological, and chemical nanoparticle transformations during selected heterogeneous and electrochemical reactions, integrate them into the current state of knowledge, and discuss important future developments.

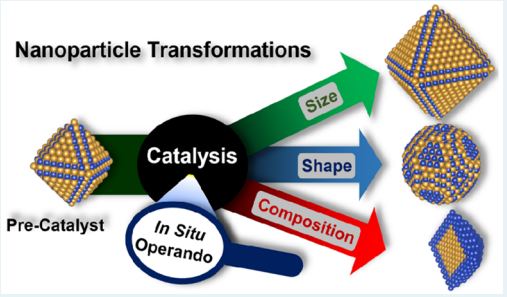

KEYWORDS: *operando, in situ, nanoparticle, catalysis, electrocatalysis, X-ray, spectroscopy, microscopy*

1. INTRODUCTION TO IN SITU AND OPERANDO INVESTIGATION OF NANOCATALYSTS

One of the greatest impacts of catalysis research on humankind was the development of the Haber−Bosch process more than 100 years ago to produce ammonia for fertilizers on an industrial scale, as it contributed to increase the world food production.[1,2] Today, catalysis research involves various disciplines ranging from surface science investigations of atomically flat or tailored single crystal surfaces[3] and nanoparticles,[4] to engineering disciplines optimizing reactor design and operation for large-scale facilities in the chemical industry. Nevertheless, independently of the length scale in which the catalyst has to be operated or studied, the design of an optimized catalyst for improved efficiency, stability, sustainability and low cost demands extensive knowledge of the catalyst system under operando reaction conditions. Here, the structural/chemical evolution and deactivation under stationary as well as varying operating conditions must be known to estimate or predict the catalyst lifetime. Varying the operating conditions is especially relevant for (electro)-chemical energy conversion processes to store intermittently provided electrical energy from renewable power sources. In many cases, the key to operate industrial scale facilities efficiently and cost effectively is not to achieve peak activity marks but to increase the catalyst lifetime.[5]

At this stage, in situ and operando insights into nanocatalysts is of utmost importance, as here (varying) reaction conditions can be simulated while providing information on the nanocatalyst structure, morphology, composition, and chemical state under reaction conditions. The overall goal of identifying decisive properties for catalysts including the active sites under operating conditions, remains. It should be kept in mind that the as-prepared materials are only precatalysts that become activated under reaction conditions, often through drastic structural/chemical modifications. Therefore, efforts that have been undertaken in the past to correlate physicochemical properties of the as-prepared catalysts to a particular activity/selectivity trend must be redirected toward those that take into consideration the transformations that the active catalyst has undergone to adapt to the specific reaction conditions.

In this review, we discuss recent findings on in situ transformations of nanoparticles during heterogeneous gas-phase catalytic and electrocatalytic processes. Studies based on various experimental techniques are presented, such as in situ scanning and transmission electron microscopy (SEM and

Received: May 3, 2019
Revised: July 29, 2019
Published: August 30, 2019

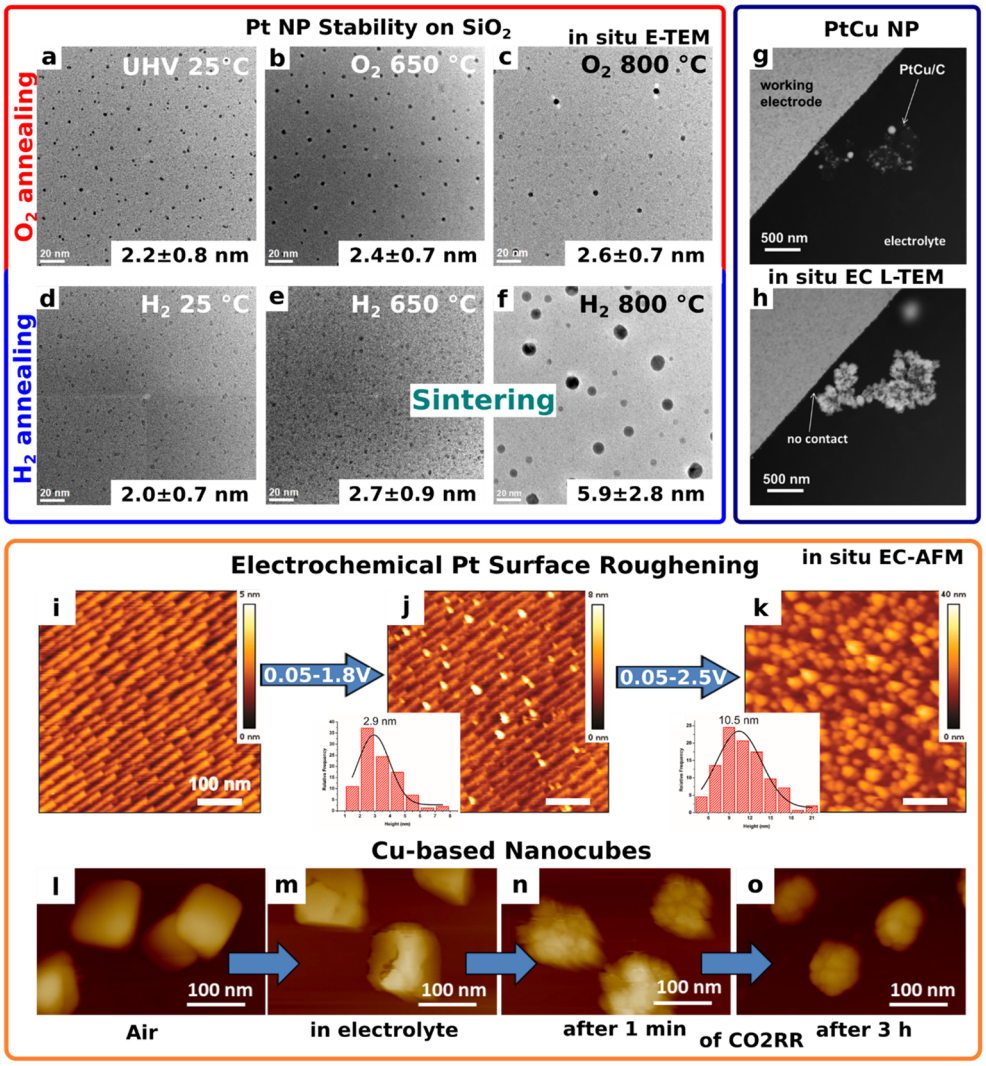

Figure 1. Mobility and sintering of size-selected Pt NPs on SiO_2 monitored under vacuum (a) and at 1.33 mbar under an O_2 (b, c) and H_2 (d–f) atmosphere by using in situ E-TEM at elevated temperature. (g, f) Evolution of carbon-supported PtCu NPs under electrochemical conditions before and after potential cycling, respectively, as studied via in situ electrochemical liquid-phase TEM. (i–k) Pt surface roughening and Pt NP formation under electrochemical potential cycling in 0.1 M H_2SO_4 and the corresponding height distributions. (l–o) Morphological evolution of Cu-based nanocubes (l) in the as-prepared state, (m) immersed in the 0.1 M $KHCO_3$ electrolyte, and (n, o) during CO_2 electroreduction (CO_2RR). (a)–(f) are reproduced from ref 12 with permission from the PCCP Owner Societies. (g)–(h), (i)–(k), and (l)–(o) are reproduced with permission from figures in refs 12, 17, 39, and 40, respectively. Copyright 2016, American Chemical Society, 2018 Wiley-VCH, and 2018 American Chemical Society, respectively.

TEM) applied under a gas-phase (E-) or liquid (L-) environment or scanning probe microscopy (e.g. atomic force microscopy (AFM)) to identify morphological and structural transformations. In situ X-ray-based techniques are presented, showing changes in the chemical state as well as in the local atomic structure via X-ray absorption near-edge structure (XANES) and extended X-ray absorption fine structure (EXAFS) spectroscopy. Insights into morphological and structural transformations were also provided by using small angle X-ray scattering (SAXS) and X-ray diffraction (XRD) obtained for either powder samples or (epitaxial) NPs and thin films in a grazing incidence (GI) configuration. The experimental findings were supported by theoretical studies based on not only density functional theory (DFT) and thermodynamics-driven NP reconstructions, especially with respect to adsorbate-induced changes of the equilibrium NP morphology, but also ab initio molecular dynamics (AIMD) calculations. We also exemplify the importance and strength of combining structural and morphological investigations with vibrational spectroscopy such as diffuse reflectance infrared Fourier transform (DRIFT) spectroscopy[6] and Raman spectroscopy, allowing deep insight into adsorbate-induced NP modifications. Additionally, simultaneous product analysis using gas chromatography (GC) or mass spectrometry (MS) converts in situ into operando investigations.[7] In this manner, correlations between reaction mechanism/pathways and NP transformations can be established. Compositional changes, especially of the catalytically most relevant near-surface, are discussed on the basis of near-ambient-pressure (NAP) X-ray photoelectron spectroscopy (XPS).

In this work, relevant catalytic processes from an academic and industrial point of view, involving the activation of small molecules, are discussed, such as the oxidation of CO, H_2O, and NO and the reduction of CO_2 and NO. Our review addresses mainly transformations of nanoparticle catalysts taking place under (near-)ambient-pressure conditions,

DOI: 10.1021/acscatal.9b01831
ACS Catal. 2019, 9, 10020–10043

although in sections where a limited number of such studies are available, some selected examples are also given involving lower pressures. In section 2 we focus on morphological transformation with respect to the NP size and shape under oxidizing and reducing reaction conditions. In section 3, we discuss the (bulk) chemical state and near-surface structure transformations followed by a summary of most recent studies on compositional changes and surface segregation[8] in NPs under reaction conditions. Finally, in section 4 we discuss challenges that catalysis research faces today and how these may be tackled in the years to come.

2. MORPHOLOGICAL CHANGES IN NANOPARTICLES UNDER REACTION CONDITIONS: SIZE, SHAPE, SINTERING, AND REDISPERSION

2.1. Size Modifications of Nanoparticles under Adsorbate Exposure and Catalytic Reactions. Designing heterogeneous catalysts with improved catalytic performance involves being able to achieve a high density of catalytically active sites, which in a first approximation correlates with its physical surface area. Thus, nanostructuring is a typical pathway employed for catalyst optimization to increase the surface to volume ratio and mass-based surface area. In contrast, in a number of cases, catalyst degradation correlates with the growth of the nanoparticles under catalytic conditions, which is accompanied by the loss of surface area and active site density.[9] In situ techniques such as TEM,[10−20] XAFS,[21−25] XRD,[26−29] and SAXS[30−36] have been used to monitor the growth of metal NPs under gas-phase thermal catalysis and electrochemical reaction conditions, as seen in the in situ TEM images of Figure 1.

A versatile approach to study morphological transformations in nanocatalysts is to utilize size-controlled NPs homogeneously distributed on a support, since this allows the researcher to more easily investigate sintering and redispersion processes.[37] For small NPs and clusters, changes in their size and shape directly influence the mean coordination number (CN) of the nearest metal−metal distances in the NP.[38] Such modifications can be tracked via in situ/operando EXAFS, a technique that has been applied to various noble-metal catalysts such as Al_2O_3-supported Pt NPs during thermal NO oxidation[21] and Pd NPs during NO/CO cycling[22] as well as during NO reduction conditions.[23] Similarly, the NP growth under electrocatalytic conditions has been reported during electro-oxidation of isopropyl alcohol for Au NPs.[24]

In some cases, sintering was studied using in situ TEM.[10−18] For example, the temporal evolution and dynamics of particle growth was shown for Pt NPs supported on zeolites under a variety of reaction conditions (CO oxidation, NO reduction via CO or H_2, water-gas shift reaction).[18] The mobility and morphological stability of size-selected Pt NPs synthesized by inverse micelle encapsulation on SiO_2 thin films was also investigated (Figure 1a−f).[12] The ∼2.5 nm large preoxidized Pt NPs were exposed in situ to 1.33 mbar of either pure O_2 or pure H_2 from 25 to 800 °C. Under oxidative conditions the NPs do not show any sintering up to 450 °C, while above 650 °C the formation of small PtO_x clusters coexisting with larger NPs is assigned to a redispersion phenomenon favored by the formation of volatile PtO_x species (Figure 1b). An additional decrease in the NP size is observed upon further annealing in O_2 at 800 °C, suggesting the loss of material (via pumping in the E-TEM, Figure 1c).

In clear contrast, increasing the temperature under H_2-containing conditions up to 650 °C leads to PtO_x reduction (Figure 1e) and drastic sintering at 800 °C via NP diffusion-coalescence (Figure 1f), also leading to 4−5 nm Pt_3Si NPs through NP/support (Pt NP/SiO_2) interactions, as revealed by electron diffraction. Interestingly, subsequent exposure of the redispersed PtO_x to H_2 at 450 °C resulted in reagglomeration and larger metallic Pt NPs. The formation of Pt_3Si can be explained by the decomposition of SiO_2 regions in the proximity of Pt NPs, leading to the direct interaction of the Pt NPs with Si from the support, which enables silicide formation. A similar process was identified for Au NPs which dig vertical channels into a SiO_2 support at temperatures up to ∼1000 °C under UHV conditions, as revealed by AFM.[41] We note that, in the Pt/SiO_2 study, special care was taken to minimize the influence of the electron beam. This work especially illustrates the power of HRTEM studies in combination with electron diffraction to reveal not only morphological but also structural adsorbate-driven NP transformations and sintering phenomena.

Among the in situ XAFS studies,[21−24] a combinatory study applying DRIFTS and mass spectrometry gave especially comprehensive insights into the dynamic changes of the size and dispersion of Pd NPs supported on $CeO_2/ZrO_2/Al_2O_3$ during alternating reaction conditions.[22] On switching from a CO- to a NO-containing atmosphere at 400 °C and 2 bar, the initially oxidized Pd NPs reduce in the presence of CO under CO_2 evolution, forming a CO-covered Pd NP surface. Introducing NO initiates the Pd NP redispersion on the support, while CO adsorbates get catalytically converted to CO_2 and N_2 via NCO adsorbates as well as N and O species. After full conversion of the C-containing adsorbates, the Pd NPs oxidize in the presence of NO. Switching to a CO-containing atmosphere initiates the Pd NP sintering and the described cycle restarts. Oscillations of the Pd NP size within the cycle were determined from the Pd−Pd coordination numbers extracted from the in situ EXAFS data. This study nicely shows how dynamic processes and the mechanisms of chemical transformations can be revealed by concurrently tracking adsorbates via vibrational spectroscopy, reaction products via mass spectrometry, and structural/morphological transformations via XAFS.

We have to note that in situ/operando studies based purely on either local (SEM, TEM) or ensemble-averaging methods (XAFS, XRD) do not necessarily yield the correct global picture of the NP catalyst. In the case of microscopy methods, deep atomistic insight may be obtained from a spatially limited and not necessarily representative fraction of the sample. On the other hand, averaging spectroscopy and diffraction methods may result in wrong structural/chemical information if the NP properties are heterogeneous (lack of narrow size, shape, and composition distribution). In the case of XRD, approaches in data analysis can be applied that can account for and quantify asymmetric size distributions, as shown for Cu NPs on ZnO.[42] An elegant way to overcome these difficulties for NP catalysis research is to combine both local and statistical in situ/operando methods, yielding a more complete picture of the complex NP catalysts. This has been shown for instance for supported Pt NPs during ethylene hydrogenation[43] as well as CO oxidation in the presence of propene simulating the conditions of a diesel exhaust atmosphere.[44] In the former work, a universal microreactor that can be applied for STEM and XAFS experiments at a gas pressure of 1 atm

DOI: 10.1021/acscatal.9b01831
ACS Catal. 2019, 9, 10020−10043

was developed. The separate experiments can be linked by the product analysis that was conducted simultaneously. With this approach, it was revealed that the catalyst consists of atomically dispersed Pt species as well as NPs above 1 nm size in an ethylene-rich gas feed (H_2:C_2H_4 ratio of 1:3). The atomically dispersed Pt species were not detectable by STEM, which solely revealed the growth of the NPs, but Pt redispersion on the support was identified using XAFS.[43] In the latter work, the dynamics of the Pt NP redispersion on a CeO_2 support during an oxidative pretreatment, reductive activation, and CO oxidation catalysis was investigated using operando XAFS combined with E-TEM.[44] Similarly, the Pt NPs redisperse under an oxidative treatment at 500 °C and Pt NPs form under reductive atmospheres at 250 °C. Most importantly, the combined investigation leads to the identification of an optimized pretreatment procedure of the Pt NPs during which the propene concentration was cycled in a reductive activation step.

With respect to electrocatalytic conditions, significant morphological changes of NPs have been recently reported during electrochemical reactions via for example electrochemical AFM, STM, and scanning electrochemical microscopy (SECM).[39,40,45] In situ electrochemical L-TEM is technically more challenging and is not yet fully established, as there have been only a few studies of NPs under electrochemical conditions.[16,17,46] Recently, the degradation pathways of octahedrally shaped PtNi NPs during electrochemical potential cycling were investigated using in situ electrochemical L-STEM.[18] Therein, NP dealloying via Ni dissolution could be followed and quantified in the initial potential cycles. After Ni dealloying, the mobility and coalescence of the NPs during carbon corrosion conditions was the main structural modification observed, which was less severe under potential cycling in comparison to constant potential conditions. At constant high electrode potential, NP sintering via a facet-to-facet attachment was found to occur within 10 s. Additionally, the degradation of FePt NPs during the electrochemical oxygen reduction reaction was studied via electrochemical L-TEM under conditions that mimic fuel cell operation.[16] During electrochemical potential cycling, an increasing density of NPs on the carbon support was found as well as the formation of chain- or dendrite-like structures. Additionally, carbon corrosion as well as a potential-dependent variation of the particle size was revealed. This work shows the possibilities but also indicates the experimental difficulties, as reflected in the inhomogeneity of the processes due to local changes in the conductivity, as well as the possible effects of the electron beam itself, which are still largely unknown. In a different study, a surprisingly strong NP growth was observed under supposedly electrochemical conditions in a case when the NPs lost electric contact to the substrate (Figure 1g,h).[17] Notably, areas which remained electrically connected did not exhibit this large particle growth, indicating a very significant beam-induced particle growth. Nonetheless, we expect that the field of electrochemical L-TEM will continue to develop rapidly in the near future, allowing researchers to gain more in-depth insight into NP growth, dissolution, and shape modifications under electrochemical conditions provided that the many technical and experimental issues currently faced by researchers in this field can be satisfactorily resolved. As a compromise for a real electrochemical flow cell configuration, insights into the morphological transformation of Pt NP fuel cell catalysts supported on carbon were gained using E-TEM under an O_2 and H_2O atmosphere.[15] Therein, it was shown that the mobility of NPs leads to a particle growth via coalescence, which is preceded by a NP rotation to align the lattice planes of the individual NPs. It should be considered that any in situ TEM investigation should be benchmarked against the already successful identical location-TEM approach,[47−50] as well as alternative methods such as in situ (GI)SAXS studies.[32−35,51] For example, an in situ SAXS study nicely revealed the growth of Pt NPs under electrochemical potential cycles simulating fuel cell operating conditions.[51] Almost simultaneous in situ XAFS experiments (the spectra were recorded in the same setup within a couple of minutes) showed that the Pt−Pt distances within the Pt NPs increased as the particle size grew.

Utilizing in situ electrochemical scanning probe techniques, the reversible electrochemical formation and dissolution of Pt NPs on electropolished Pt could also be demonstrated with EC-AFM (Figure 1i−k).[40] The Pt surface was found to resist morphological transformations under mild electrochemical potential cycling. Increasing the upper potential limit up to 1.8 and 2.5 V leads to the formation of Pt NPs with mean heights of ∼3 and ∼10 nm, respectively. Similarly, the electrochemical roughening and nanoisland formation during potential cycling was studied on Pt(111) using EC-STM.[52]

As CO_2 electroreduction (CO_2RR) has received increasing attention in catalysis research in recent years and the majority of works utilize Cu-based electrocatalysts,[53−56] the morphological transformation of Cu-based nanocubes (NCs) during CO_2RR was tracked using in situ EC-AFM and in situ XAFS.[39] The electrochemically prepared NCs were synthesized between ∼200 nm and ∼1 μm. Exposing the NCs to the electrolyte induced the formation of cracks on their surface. Already after 1 min under CO_2RR conditions the NC size and morphology strongly changed (see Figure 1l−o). The cube edge length decreased by ∼10%, and the NC became smeared out. After three additional hours of electrocatalytic operation, the NCs appeared rather spherical and their size decreased again by about 10%. In the case of larger NCs, a pore structure became visible. In situ XAFS measurements showed that the size changes are linked to the reduction of the NCs to metallic Cu under the reaction conditions as well as the loss of Cl when the NCs are first introduced into the electrolyte, even in the absence of an applied potential.

The former in situ electrochemical AFM studies nicely illustrate the capability of the technique to track the morphological changes of well-defined surfaces and individual NPs under electrochemical and electrocatalytic conditions. From here on, the in situ combination of scanning probe techniques with optical, vibrational, or X-ray spectroscopy methods under electrochemical conditions will give a more comprehensive picture.

2.2. Shape Transformations of Nanoparticles under Reaction Conditions. In addition to the changes in the particle size, shape modifications of NP catalysts can tremendously influence the catalytic activity, as the active site might be linked to a certain defect motif or preferred surface termination.[57] It is well-known that the growth direction of NPs from clusters can be controlled by the adsorption of molecules such as CO, leading to sophisticated particle morphologies.[58] Heterogeneous catalysis, however, is based on the adsorption of molecules as either reactants or intermediates, which can affect the morphology (as well as surface composition) of nanocatalysts under reaction con-

DOI: 10.1021/acscatal.9b01831
ACS Catal. 2019, 9, 10020−10043

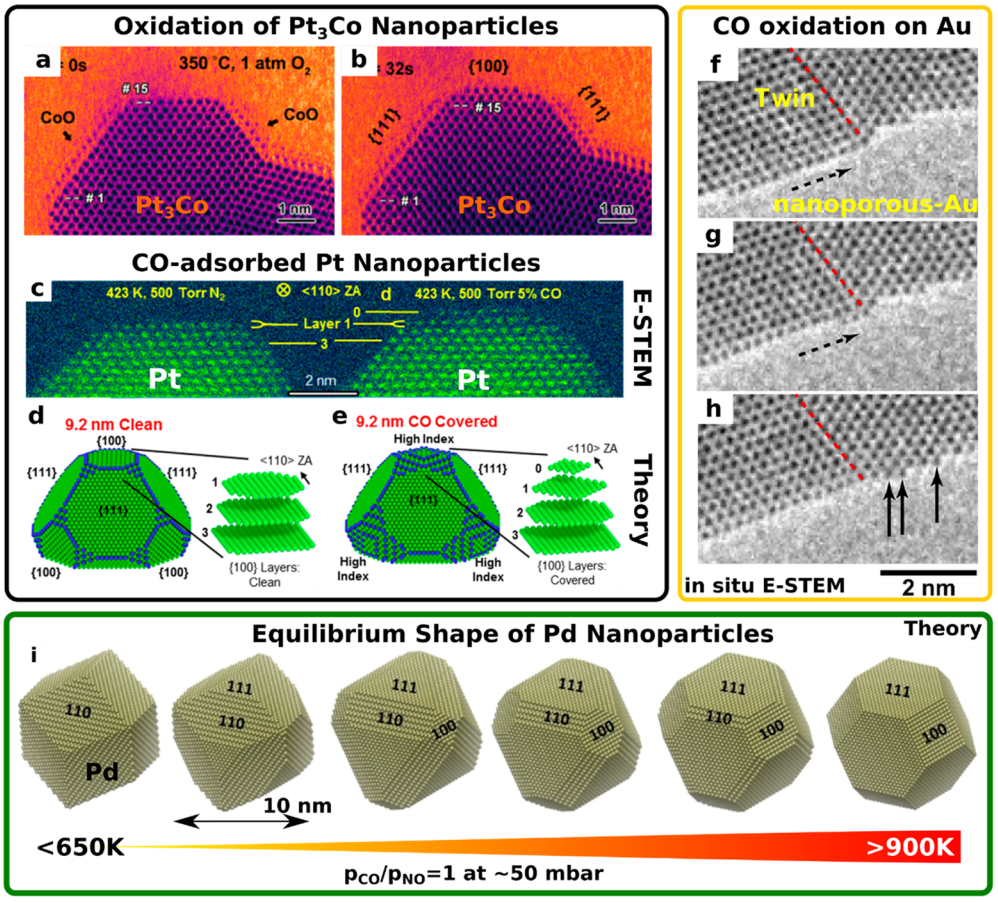

Figure 2. (a, b) In situ cross-sectional STEM images showing the shape changes of a Pt_3Co NP under an oxidative treatment at 350 °C. (c–e) Morphological change of the (100) facets of a truncated Pt octahedron NP during CO adsorption at elevated temperature (~127 °C) extracted from in situ STEM images (c). Models depicting the equilibrium shape as determined based on DFT calculations are also shown (d, e). (f–h) In situ E-TEM images of nanoporous Au showing the mobility of Au atoms under CO oxidation conditions in the vicinity of twin boundaries. (i) Calculated equilibrium shape of Pd NPs in the presence of CO and NO at various temperatures. The figure was reproduced/adapted with permission from refs 63–66. Copyright 2017, 2017, 2014, and 2018, respectively, American Chemical Society.

ditions. Not only the most stable surface termination but also the number of edges and corners can be decisive for the catalytic function.[59,60] In this respect, the nearest-neighbor approach takes into account the catalytic activity of distinct metal adsorption sites by their coordination environment. A generalized coordination number can be formulated for each site by counting the number of atoms in the first coordination shell weighted by their deviation from the expected ideal coordination environment, such as a coordination number of 12 for a metal atom in the face-centered-cubic structure. This generalized coordination number was found to be correlated to the catalytic activity of distinct terminations and defect motifs of metal surfaces and NPs.[61,62]

On the basis of the nearest-neighbor approach, the influence of the ensemble of sites on Pt NPs of various shapes on the overall CO oxidation kinetics has been investigated by kinetic Monte Carlo simulations.[67] The authors showed that the kinetic coupling between surface sites, e.g. on the NP edges between (100) and (111) facets, has to be taken into account and that isolated active sites are not sufficient to describe and explain the catalytic activity of a NP. Generally, a wide distribution of surface sites seems beneficial for the CO oxidation catalysis according to these theoretical calculations.

Shape transformations of NPs and, especially, adsorbate-induced phenomena have been investigated using not only experimental techniques such as in situ E-TEM but also theoretical calculations or combined studies.[20,59,60,63−66,68−81] For example, the shape change of a Pt NP (~20 nm) on changing from reducing (H_2) to oxidizing (O_2) conditions in the millibar regime was experimentally studied using E-TEM.[69] In vacuum and under an H_2 atmosphere, the NP morphology is close to the equilibrium (Wulff) shape of a truncated octahedron, but changing to an O_2 atmosphere leads to a roughening of the (111) facets between the (100) facets. These changes decrease the (111)/(100) ratio of facets and leads to a rounded morphology. In contrast, an in situ STEM study in a gas cell at 1 bar of O_2 pressure at 350 °C revealed a facet-dependent oxidation of Pt_3Co NPs.[65] Figure 2a,b, the Pt-terminated (100) facet restructures, forming low-coordination sites within less than 1 min, whereas the CoO-terminated (111) facets retain their atomically flat termination. The Co–O termination of the (111) facets results from a lower surface free energy, as determined by DFT calculations.

The morphology of pure Pt[63,70] and pure Au NPs[20,71,72] was investigated under CO oxidation conditions. In the case of the pure Pt NPs, the truncation of the as-prepared octahedron decreased in the presence of a CO-covered surface above 127 °C, as revealed by a combined in situ STEM and DFT study.[63] In contrast to the O_2-containing atmosphere described above ($CO + O_2$), the Pt(111) facets remain intact when CO

DOI: 10.1021/acscatal.9b01831
ACS Catal. 2019, 9, 10020−10043

is adsorbed, but the (100) facets were roughened into stepped (210) and (310) facets, Figure 2c. The higher index facets exhibit a lower surface free energy at high CO coverages in comparison to the (100) and (111) facets, and the shape determined was confirmed by theoretical calculations (Figure 2d,e).

In a different in situ TEM study, an oscillatory morphology change of Pt NPs involving a dynamic refaceting at ∼450 °C was revealed using a micro flow reactor which allows studies at 1 bar and elevated temperatures with simultaneous detection of the reaction products.[70] The fraction of the (111) facets on the Pt NP constantly alternates, leading to an oscillation between a rather faceted and a rather spherical NP morphology. In parallel, the reaction rate of CO oxidation oscillates, as revealed by calorimetry and reaction product analysis. This work furthermore shows that combined operando studies also tracking reaction products are especially important for an in-depth understanding of the reaction mechanisms in nanocatalysis.

In the case of CeO_2-supported Au NPs under stationary CO/air conditions, a reconstruction of (100) facets was determined at 0.45 mbar and room temperature because the outermost atomic layers form an undulating hexagonal lattice with shorter lateral Au−Au distances.[20,71] Additionally, a decreasing CO partial pressure in air (3 mbar) led to a gradual loss of faceting of the Au NP from a polyhedral shape in a CO/air mixture to a spherical shape in air.[71] A study of the dynamics of Au NPs/CeO_2 combining E-TEM and theoretical calculations revealed that under CO/O_2 gas mixtures the 4 nm NPs reconstruct, whereas smaller Au NPs (<2 nm) decompose, leading to single-site AuCO species on the CeO_2(111) surface.[72] The fast dynamics of the AuCO extraction process was simulated using DFT and ab initio molecular dynamics (AIMD) calculations and showed that 2D clusters transform within 25 ps to 3D clusters. In this study, the influence of the beam dose rate effect on the dynamics of the restructuring was considered. Generally, the presence of the electron beam during the experiment is expected to be detrimental to the adsorption of CO on the NP, since it gives rise to an electron energy transfer leading to CO desorption and/or a knock-on mechanism.

The mobility of surface atoms under reaction conditions was additionally shown for nanoporous gold.[64] Nanoporous Au is an important model system in catalysis research simulating Au NPs and enables the study of selected structural and morphological transformations on sub-nanometer and atomic length scales during catalysis. Due to the absence of NP mobility in nanoporous Au, these in situ experiments can be performed in greater depth in comparison to those on supported Au NPs. An atomic motion of Au along surface steps only occurred under CO oxidation conditions, but not in the pure gases or under vacuum. Thus, it was concluded that such motion was caused by the generated heat of reaction. Interestingly, planar defects in the Au lattice such as twin boundaries that reached the surface of a nanopore were found to limit the atomic motion, Figure 2f,h, leading to a preferred growth of the nanopores. This study nicely demonstrates how atomic insights extracted from in situ electron microscopy can contribute to the improvement of the catalyst design by tailoring structural and morphological properties.

Shape changes of NPs have been predominantly investigated using advanced microscopy methods, but morphological modifications can also be assessed by X-ray scattering and diffraction techniques. Although these X-ray-based techniques rely on structural models and a fitting procedure in contrast to the direct assessment of the NP morphology in microscopy, they are highly important due to their more straightforward utilization as in situ or operando methods under more realistic conditions at higher temperatures and pressures. For example, Rh NPs have been investigated using in situ surface X-ray diffraction under O_2 dissociation and CO oxidation conditions.[82] Therein, it was shown that the epitaxial Rh NPs supported on Mg(001) reversibly change their (001)/(111) faceting ratio. O_2 dissociation at 327 °C led to the growth of the (001) facets, whereas CO oxidation was accompanied by a growth of the (111) facets. The NP size was found to remain stable, but the formation of an O−Rh−O surface termination was confirmed by ex situ HRTEM.

In addition to the experimental studies, theoretical calculations have been widely applied to predict the shape changes of NPs induced by specific adsorbates and/or under reaction conditions. These theoretical studies are mostly based on first-principles calculations, e.g. of the surface free energies using DFT, and Wulff−Kaichew constructions. These calculations yield the equilibrium shapes of NPs as well as smaller clusters and have been applied to oxides and metals not only under noncatalytic[72−76] but also under reaction conditions.[66,76−81] These theoretical studies allow a straightforward variation of the reaction conditions in comparison to the experimental studies and can lead to predictive statements: e.g., on the catalyst stability.[83] The equilibrium shapes of metal NPs such as Cu, Pd, Pt, and Au have been investigated in various (reactive) gas atmospheres such as NO, CO, and H_2O by applying a multiscale structure reconstruction model which combines Wulff−Kaichew constructions, Langmuir adsorption isotherms, and DFT.[66,80,81] For example, Meng et al. studied the equilibrium structures of 10 nm Pd, Pt, and Rh NPs in CO- and NO-containing gas mixtures at various pressures and temperatures (Figure 2i).[66] The calculations showed not only that the temperature and pressure determine the NP shape but also that an increasing NO content leads to a growing fraction of (110) facets, while the fraction of (100) and (111) decreases. In a more recent study, the interplay between Cu NP and the ZnO support as well as between Pt NP and $SrTiO_3$ support was taken into account[78] and contrasted with experimental findings based on in situ E-TEM.

These studies exemplify the morphological evolution of NPs under reaction conditions and how theoretical calculations can contribute to the understanding of such transformations. For example, they show how NPs with certain surface terminations can be rationally designed and tailored by exposing them to specific adsorbates.

Unfortunately, the high number of atoms involved in NP−support ensembles limits the extent of calculations that can be performed because of the high costs of the theoretical calculation. Therefore, many theoretical studies of NP−support ensembles consider metal (oxide) clusters on a few monolayers of support material.[62,72,79,83,87−92] In this respect, it was shown that the surface terminations of the (100) and (110) facets of the γ-Al_2O_3 support under reaction conditions determine the most stable morphology of Pd_{13} and Pt_{13} clusters.[79] On the bare γ-Al_2O_3(100) surface, a biplanar cluster is favored, whereas surface 3D-like clusters are more stable on the partially hydroxylated γ-Al_2O_3(110). Experimentally, similar trends have been found for Al_2O_3-supported Pt_{22} clusters studied at various H_2 pressures by using in situ

DOI: 10.1021/acscatal.9b01831
ACS Catal. 2019, 9, 10020−10043

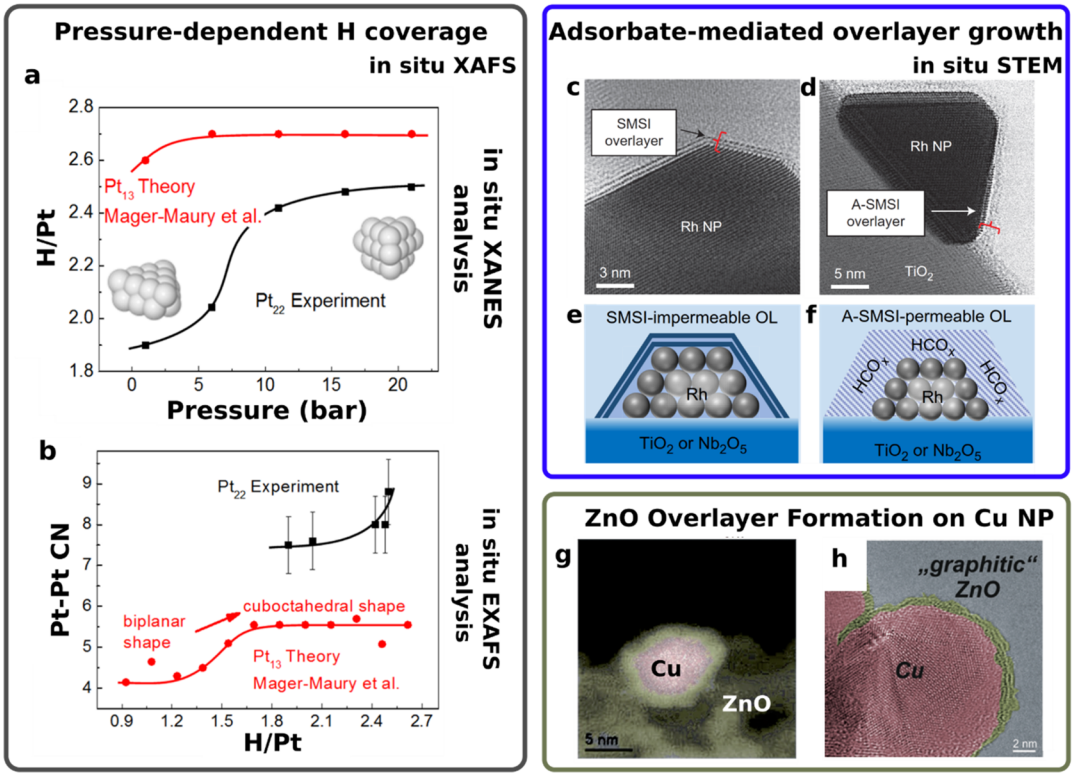

Figure 3. (a, b) Evolution of the morphology of Pt NPs depending on the H coverage as determined by in situ XAFS analysis and theoretical calculations. The experimentally determined H surface coverage on Pt_{22} NPs and theoretically determined for Pt_{13} NPs is shown in (a). In (b) is shown the correlation between the H coverage and the NP shape as determined from the analysis of Pt−Pt nearest-neighbor coordination numbers of in situ XAFS spectra together with analogous information extracted from DFT for Pt_{13} NPs. (c−f) The formation of adsorbate-mediated overlayers on Rh NPs supported on TiO_2 or Ta_2O_5 during reductive pretreatment of these CO_2 hydrogenation catalysts. In (c) and (d) are shown in situ STEM images recorded at atmospheric pressure after the reductive pretreatment. (e, f) Visualization of the morphological evolution of the NP-support ensemble after 4 h at 250 °C in CO_2/H_2 = 10 and 1 h at 500 °C in H_2, respectively. (g, h) Formation of metastable "graphitic" ZnO overlayers on a Cu NP occurring after a reductive pretreatment of industrial $Cu/ZnO/Al_2O_3$ catalysts for methanol synthesis. (a)−(b), (c)−(f), and (g)−(h) are reproduced and adapted with permission from figures in refs 84−86, respectively. Copyright 2014 Wiley-VCH, 2017 Springer Nature, and 2015 Wiley-VCH, respectively.

XAFS, Figure 3a,b.[84] Increasing the H_2 pressure up to 21 bar led to an increased H surface coverage on the Pt NPs that resulted in a 2D to 3D shape transformation, as concluded from the increased Pt−Pt CNs.

In all in situ and operando investigations, the influence of the probing method should be considered and minimized as much as possible. This is especially valid for in situ TEM investigations, as already pointed out for the electrochemical L-TEM studies. For example, in the case of manganites under E-TEM conditions, cationic movement was revealed during electron bombardment.[93] Drastic morphological and structural changes can be induced by the electron beam. For instance, Co NPs were found to oxidize under 0.2 μbar of oxygen at 300 °C only under electron beam irradiation.[94] Irradiating the metallic Co NPs (~20 nm), which were covered by graphite layers, with an electron beam at various intensities led to the formation of hollow Co_3O_4 NPs. The initial stages of the oxidation showed cracking of the graphite followed by the diffusion and oxidation of the Co atoms to CoO domains. This oxidation initiates the migration of Co atoms and the formation of cavities within the particle. Prolonged illumination was found to increase the size of the cavity, leading to a shell thickness of ~4 nm after 20 min. The Co NP was also found to oxidize at room temperature under electron irradiation, but with a significantly lower rate. These studies exemplify the effect that the electron beam can have on NPs and highlights the importance of differentiating between the electron beam induced effect and changes induced by the nonambient conditions during in situ E-TEM experiments. However, also in the case of Cu NPs, the formation of hollow Cu_2O NPs under ambient ex situ conditions was found.[95,96]

In addition to shape changes of the NP catalyst itself, the interaction between two (NP) phases can lead to significant morphological changes under reaction conditions. A prominent process is the strong metal−support interaction (SMSI), during which a typically reducible material such as ZnO, CeO_2, TiO_2, or Fe_3O_4, usually present as a support, grows above the primary NPs, forming an overlayer and changing the NP shape significantly.[85,86,97−99] This shape transformation and modified surface composition can have a favorable or a detrimental effect on the catalytic function of the primary NP.[100] The SMSI has been investigated in the case of high-pressure CO_2 hydrogenation catalysts such as $Cu/ZnO/Al_2O_3$ and Rh NPs deposited on TiO_2. High-pressure CO_2 hydrogenation is the industrial process to produce methanol. One of the pioneering works on E-TEM for the investigation of NP catalysts was performed on Cu NP supported on ZnO/Al_2O_3.[10] In the as-prepared state, the catalyst NPs consist of CuO, which have to be activated by a reductive treatment prior to catalytic operation. During this activation treatment the CuO_x domains were found to interact with the ZnO, leading to a graphite-like ZnO overlayer on the Cu NPs.[86] These overlayers are in

DOI: 10.1021/acscatal.9b01831
ACS Catal. 2019, 9, 10020−10043

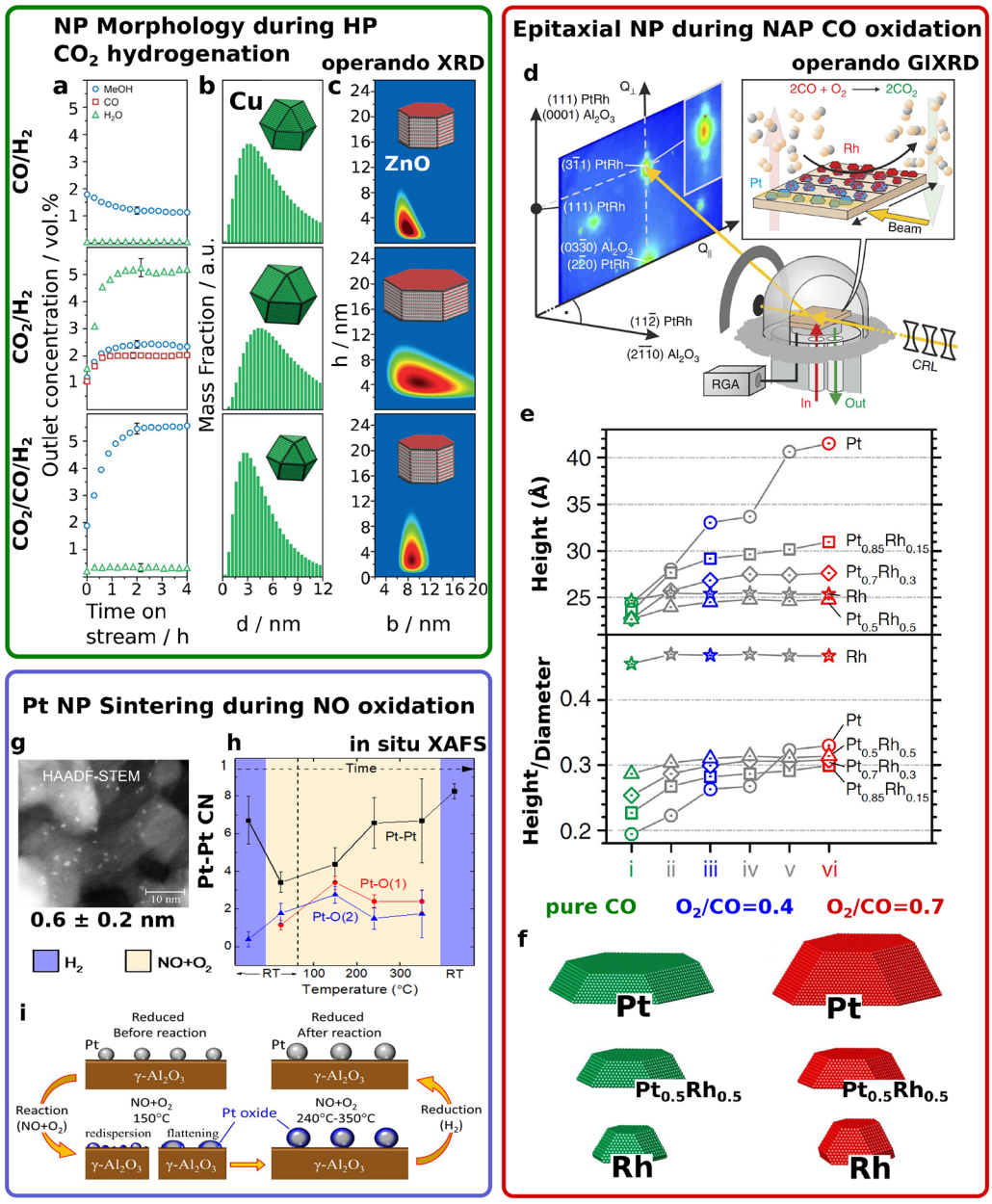

Figure 4. Evolution of the Cu and ZnO NP morphology during high-pressure (HP) CO_2 hydrogenation under CO/H_2, CO_2/H_2, and $CO/CO_2/H_2$ feed gas compositions, as extracted from Debye analysis of operando X-ray powder diffraction patterns. The outlet gas composition is shown in (a), the particle size distribution of the Cu NP crystallites in (b), and the mass fraction of ZnO crystallites depending on base diameter "*b*" and the height "*h*" in (c). (d–f) Sintering of epitaxial Pt_xRh_y NPs on $Al_2O_3(001)$ under NAP CO oxidation conditions as determined by operando grazing-incidence (GI) X-ray diffraction. The schematic of the experiments is shown in (d). In (e) are shown the NP height and height/diameter ratio as extracted from line scans of selected Bragg peaks. (f) Visualization of the morphological evolution of the Pt_xRh_y NPs. In (g–i) are shown the redispersion and subsequent sintering of Pt NPs supported on Al_2O_3 during gas-phase NO oxidation as determined using in situ XAFS. (g) STEM micrographs of the as-prepared state of the ultrasmall NPs. (h) Evolution of the first-nearest-neighbor Pt–Pt coordination number at various reaction conditions. (i) Summary of the structural and morphological evolution of Pt NPs during a gas-phase NO oxidation reaction. (d)–(f) are reproduced and adapted from ref 26. (a)–(c), and (g)–(i) are reproduced and adapted with permission from figures in refs 42 and 21, respectively. Copyright 2016, Wiley-VCH, 2014 American Chemical Society, respectively.

contrast to the typical wurtzite-like ZnO domains, as they consist of stacked graphene-like layers in which the Zn and O planes of wurtzite-like ZnO are merged.[101] Importantly, Zn ion migration onto the Cu NPs has been found to play an essential role in the catalytic function.[102,103] $Zn^{\delta+}$ ions act as adsorption sites for the intermediate oxygen species during CO_2 reduction, and their proximity to Cu steps formed due to stacking faults in the Cu lattice leads to high methanol yields.[102] Thus, here the SMSI effect plays a key role in the active site formation of these industrial catalysts.

However, SMSI leading to overlayer formation and NP encapsulation can also limit the accessibility of adsorption sites, as shown for Rh NPs/TiO_2 via in situ TEM using a closed gas reaction cell operating at atmospheric pressure.[85] A thermal treatment at 550 °C in H_2 leads to a compact impermeable Ti^{3+} oxide overlayer, whereas a reactant-permeable $Ti^{3+/4+}$

DOI: 10.1021/acscatal.9b01831
ACS Catal. 2019, 9, 10020–10043

oxide overlayer was formed at 250 °C in a CO_2-rich gas stream (Figure 3c–e). Adsorbed HCO_x on the support was identified by using in situ DRIFT spectroscopy, and this adsorbate was attributed to initiate oxygen vacancy formation and Ti atom migration onto the NP surface. Interestingly, the presence of the adsorbate-mediated SMSI was found to lead to CO as the main reaction product in comparison to CH_4 on the uncovered NPs.

2.3. Sintering of Nanoparticles: Temperature and Adsorbate Effects. Sintering effects of CO_2 hydrogenation catalysts were also investigated using in situ and operando methods. The morphological and structural evolution of Cu and ZnO NPs of $Cu/ZnO/Al_2O_3$ catalysts during methanol formation has been investigated by using operando neutron diffraction.[104] The catalyst morphology and the structural defects of the Cu NPs remain stable under reaction conditions, and the incorporation of reactive species in the bulk of the NP could be excluded. In a more recent study, Cu and ZnO NPs supported on Al_2O_3 were found to sinter under non-stoichiometric reaction conditions.[42] In contrast to the optimal $CO/CO_2/H_2$ conditions leading to the highest methanol yield, the Cu NPs grew slightly and isotropically in a CO/H_2 and CO_2/H_2 gas feed (Figure 4a–c). In the CO_2/H_2 feed the Cu NP growth was more prominent, and the ZnO NP also grew significantly along the hexagonal base, leading to a platelet-like morphology. The growth of the NPs was attributed to the presence of H_2O, which was detected as a reaction byproduct. H_2O was assigned to cause Cu segregation from the ZnO and thus contribute to the sintering of the NPs. Under optimal $CO/CO_2/H_2$ conditions, the water-gas shift reaction minimizes the H_2O concentration, as revealed by in situ DRIFT spectroscopy, and thus leads to the structural and morphological integrity.

In the case of the CO oxidation reaction, the sintering of Rh-based NPs of different shapes was tracked under near-ambient-pressure (NAP) conditions using operando grazing-incidence (GI)XRD with simultaneous reaction product tracking (Figure 4d–f).[26] Bragg peak maps and line scans of epitaxially grown $Pt_{1-x}Rh_x$ alloy NPs on $Al_2O_3(0001)$ were recorded under various catalytic conditions. The particle height at 277 °C increased under CO oxidation conditions in comparison to noncatalytic conditions, as extracted from the finite height (Laue) oscillations showing a composition-dependent contraction. The main findings revealed that particle sintering and the decrease in particle coverage are significantly reduced when Rh is incorporated into the Pt NPs, Figure 4d–f. Due to the lattice mismatch between the Rh-rich NP and the $Al_2O_3(001)$ support, the NP–support interface is minimized, leading to an initial rather 3D-like particle shape. This shape is closer to the equilibrium, and thus, the metal–support interaction resulted in a reduced degree of sintering. This has been previously shown in the case of CeO_2-supported NPs.[105] We note that applying GIXRD to epitaxially grown NPs can provide insights into the NP morphology under catalytic conditions and is thus a very powerful tool to track structural transformations of model NP catalysts.

Combined insights into the chemical state and local atomic structure as well as NP and domain size can be obtained from EXAFS analysis of NPs in which the surface to bulk atom ratio is sufficiently large. At a size below 3 nm of metallic NPs the metal–metal CN decreases from the bulk-like value.[38] This approach has been applied to show the morphological transition of small Pt NPs on an Al_2O_3 support under high temperatures and various gas atmospheres. Coarsening of the Pt NPs was identified in H_2, in analogy to morphological changes observed for similar Pt NPs in Figure 1d–f with in situ TEM. The coarsening of Pt NPs grown on $TiO_2(110)$ by physical vapor deposition and by an inverse micelle encapsulation route was studied using STM after various thermal treatments and pretreatments of the support.[106] It could be shown that the smaller PVD-grown Pt NPs are more strongly bound to a prereduced support and that in general the larger micellar Pt NPs display stronger resistance against sintering.

During catalysis, in situ XAFS studies have been performed on Pt NPs during the thermal oxidation of nitric oxide[21] as well as on Au NPs during electrochemical 2-propanol oxidation.[24] Ultrasmall Pt NPs with size below 1 nm were prepared on Al_2O_3 supports using the inverse micelle encapsulation route.[21] The particle size (diameter) was stable, as revealed by ex situ TEM (Figure 4g), but differences in the Pt–Pt CNs as determined from fitting EXAFS spectra were found. The discrepancy between TEM and EXAFS analysis was attributed to a different NP shape after catalytic operation. Interestingly, a change in NP morphology in an NO/O_2 stream below the catalytic onset was observed. The Pt–Pt CN was found to decrease significantly, indicating that the Pt NPs redisperse and/or flatten on the support and no significant sintering of the NPs appeared during catalytic testing. Above the onset temperature for NO oxidation (>150 °C), the Pt–Pt CN increased, indicating the formation of more 3D Pt NPs in the catalytically active state. Similarly, Au NP electrocatalysts for 2-propanol oxidation were found to sinter with increasing reaction time, which resulted in deactivation as revealed by the analysis of CNs extracted from operando EXAFS data.[24]

Furthermore, sintering of catalysts plays a crucial role in molecular (electro)catalysis research, as the formation of NPs or nanoclusters increases the heterogeneity of the catalyst and thus complicates the extraction of reliable conclusions with respect to the catalytic mechanism and the formation of the catalytically active state. There are numerous examples in the literature reflecting the longstanding discussion on the nature of the catalysis on initially molecular catalysts,[107−109] and an increasing number of methodological works on molecular (electro)catalysts has been published.[109,110] Some examples include Co-based polyoxometalates (POM) such as Co_4- and Co_9-POMs, which have been widely studied in molecular photo- and electrocatalysis.[108,111−116] In particular, the molecular integrity of Co_9-POM was confirmed under photocatalytic phosphate-free water oxidation conditions by using in situ SAXS and pair distribution function (PDF) analysis, although with increasing phosphate concentration nanometer-sized Co phosphate domains were obtained.[114,115] Similarly, NP formation was unraveled in the case of Co-based complexes with a metal-free ligand environment during electrocatalytic HER.[117] On the basis of this study, the formation of Co NPs from a $[Co(dpg)_3(BF)_2]^+$ precursor complex was studied via in situ XAFS, showing that a typical Co NP consisted of clusters as small as 1 nm in size.[118] This study shows the relevance of organometallic complexes as precursors to form single-site, NP, and nanocluster catalysts. Recently, it has been shown that NP catalysts supported on SiO_2 decorated with single-site metal ions are highly active thermal catalysts.[119−122] For instance, increased activity and selectivity toward methanol during CO_2 hydrogenation was achieved for Cu NPs on SiO_2 when $Zr(OSi(OtBu)_3)_4$ was used

DOI: 10.1021/acscatal.9b01831
ACS Catal. 2019, 9, 10020−10043

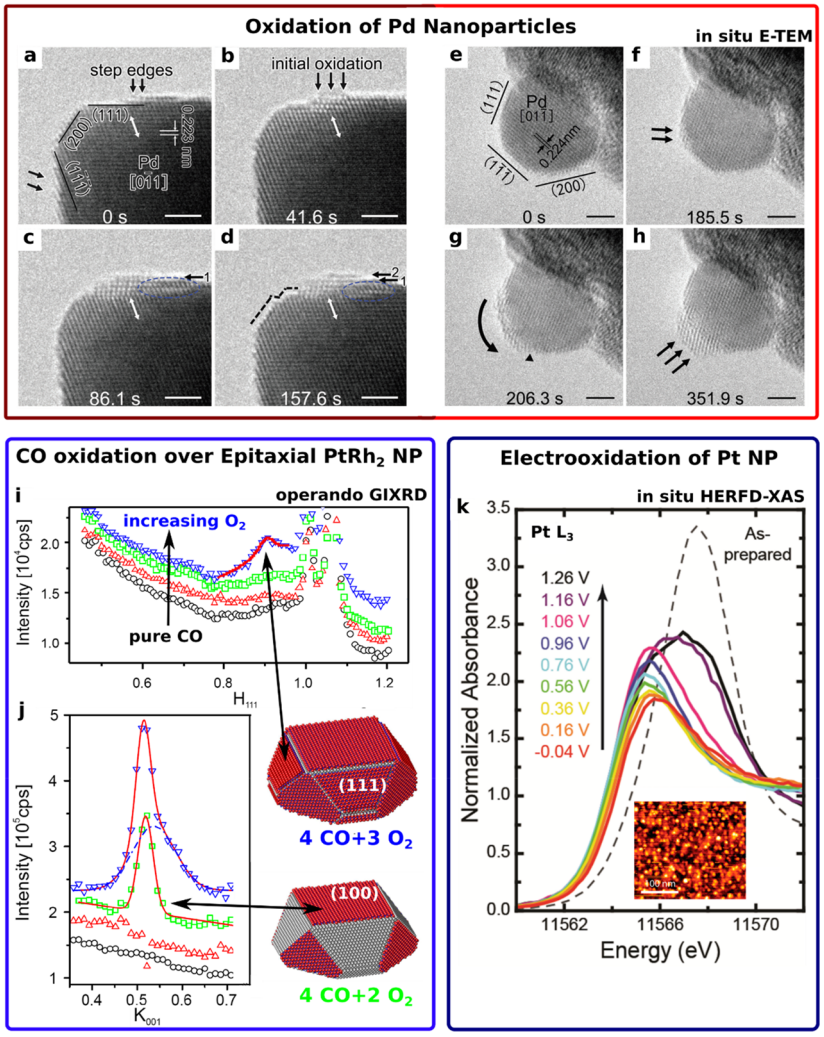

Figure 5. In situ E-TEM images of Pd NPs (a)−(d) as truncated octahedrons and (e)−(h) spheres during initial oxidation. (i, j) Operando GI diffraction peaks recorded for epitaxial PtRh NPs deposited on MgO(001) under NAP CO oxidation conditions for selected CO/O_2 gas mixtures. The proposed oxidation scheme of the NP is also depicted. (k) Initial electrochemical oxidation of size-selected Pt NPs as studied in situ by HERFD-XANES recorded at the Pt L_3-edge. An ex situ AFM image is shown as an insert. (a)−(h) and (i)−(j) are reproduced and adapted with permission from figures in ref 132 published by The Royal Chemistry Society and ref 143, respectively. (k) is reproduced and adapted with permission from figures in ref 126. Copyright 2012 American Chemical Society.

to prepare isolated Zr^{4+} sites on SiO_2.[120] Beneficial effects have also been found during methanol synthesis for Cu NPs on Ti^{4+}-modified SiO_2.[121] In the case of the Zr^{4+}-modified SiO_2, in situ XAFS revealed that the Zr sites are structurally stable under reaction conditions and do not form Zr-containing NPs or lead to Cu−Zr alloying.[120] In addition, bimetallic Ga−Pt NP catalysts prepared from single sites on SiO_2 have been shown to be highly active catalysts for propane dehydrogenation.[122] In situ XAFS showed that under reducing conditions a GaPt alloy is formed from the single sites, but a significant fraction of the Ga remains isolated on the SiO_2 surface.

These studies highlight the importance of in situ/operando investigations in the field of molecular catalysis research and the conceptual similarities to well-known electrocatalysts weakening the border to heterogeneous catalysis. We note that the same methodological pitfalls have to be considered when single-site catalysts are being prepared and investigated.

3. CHEMICAL CHANGES IN NANOPARTICLES UNDER REACTION CONDITIONS

In contrast to the morphological investigations that are most directly studied using electron or scanning probe microscopy methods, the catalyst chemical state is mostly studied using spectroscopic methods. In catalysis research, environmental, in situ/operando X-ray-based techniques have been established for many years[27,28,32,36,123−131] and thus are technologically more established than in situ/operando electron microscopy studies. Herein, XAFS in the hard X-ray regime covering 3d transition metal K-edges as well as 5d L-edges plays an important role in NP catalysis, as it can yield information on the metal oxidation state as well as metal−ligand and metal−metal distances in the coordination shells, together with providing further insight into NP−adsorbate and NP−support interactions. Furthermore, surface-sensitive diffraction as well as in situ XPS on (epitaxial) NPs can yield valuable insights into the chemical state of surface and near-surface regions, although the latter has been further developed than in situ electron microscopy.

DOI: 10.1021/acscatal.9b01831
ACS Catal. 2019, 9, 10020−10043

3.1. Chemical State and (Near-Surface) Structure of Nanoparticles under Reaction Conditions. *3.1.1. Nanoparticle Catalysts under Oxidizing Reaction Conditions.* The mechanism of NP oxidation of catalytically relevant metals for oxidation reactions such as Pd and Pt has been widely studied using in situ methods.[35,126,132−139] In the case of Pd NPs the surface oxidation of large truncated Pd octahedra (edge length of 20 nm) and spherical Pd NPs (diameter of 7 nm) was investigated in an E-TEM study, Figure 5a−h.[132] The oxidation of the Pd octahedra was found to start on the step edges of the (111) surface, leading to up to two monolayers of tetragonal PdO which then grew laterally (Figure 5a−d). The vertical growth showed a significantly lower rate, and the adjacent (100) and (1-1-1) surfaces remained unchanged. In the case of a rather spherical Pd NP, the oxidation started at the vertex sites between two (111) facets and the PdO spread on one of the (111) facets (Figure 5e−h). The oxidation might preferably start at low-coordination sites such as step edges or vertex sites and then lead to facet oxidation. Here, we have to note the differences between the oxidation of $PtRh_2$ during NAP CO oxidation conditions and the oxidation of Pd nanocrystals in an E-TEM. In the first case, the change of the surface chemical state starts from molecular oxygen, whereas in the second case it starts from O^- radicals generated by the electron beam and thus it significantly differs from the catalytic conditions. The latter highlights the importance of understanding electron-beam/environment/sample interactions and the control of the beam flux during catalysis experiments.

Within the framework of hard X-ray-based operando techniques, special configurations including grazing incidence and/or nanostructured material systems (high surface to volume ratio) can be used to overcome its large penetration depth (bulk sensitivity) and thus to gain surface insight.[21,140−143] As already pointed out above, growing NPs epitaxially on single-crystal surfaces[26,82,143] or exposing ligand-free colloidal NPs to high-temperature thermal treatments to achieve epitaxial NP/support interfaces[144] can result in atomic layer sensitivity in particle height determination under catalytic conditions with these methods.

This approach has also been used for investigating the catalytically active state of oxide-supported $PtRh_2$ NPs during near-ambient-pressure (NAP) CO oxidation.[143] Additional Bragg peaks in the reciprocal maps were identified that were attributed to the surface oxidation of the (001) facets of the NP. The formation of the O−Rh−O surface termination is accompanied by an increased CO_2 evolution rate, as determined by online mass spectrometry shown in Figure 5i,j. Here, dynamic gas-switching experiments changing the stoichiometry of CO and O_2 showed that the presence of the oxide surface termination on the (001) facets accompanies the CO_2 evolution rate, whereas the chemical state of (111) facets showed slower dynamics and was not correlated to the catalytic turnover. Interestingly, increasing the O_2 content in the gas feed from understoichiometric to stoichiometric conditions increased the CO_2 evolution rate more strongly than expected, which suggests that the reaction does not follow a simple Langmuir−Hinshelwood mechanism. Furthermore, driving the reaction under overstoichiometric O_2 conditions, which induces the oxidation of the (111) facets, did not increase the catalytic turnover. Thus, it was discussed that the dominating catalytically active sites are not located on the NP facets but at metallic sites at edges and corners presumably adjacent to the oxidized PtRh(001) facets that could lower the CO oxidation barrier. This work furthermore elucidated the need of combined structural and reaction product characterization to gain insights into catalytically relevant structural motifs.

In the case of NO oxidation over small but differently shaped Pt NPs,[21] the degree of Pt oxidation as determined by in situ XAFS analysis was found to be correlated with the catalytic activity. The Pt NPs were found to be oxidized above the onset temperature for NO oxidation (>150 °C), and a fraction of PtO_x remains present in the catalytically active state also at higher temperatures. Comparing their degree of oxidation with their catalytic properties revealed that the lower fraction of PtO_x present for the NPs with 3D-like rather than 2D-like morphology yields a higher conversion and rate constant. Thus, Pt oxide formation deteriorates the catalytic conversion of NO.

In electrocatalysis, Pt-based NPs play an important role as fuel cell catalysts due to their high activity for the hydrogen evolution reaction and oxygen reduction reaction (ORR). In the case of the ORR, the formation of Pt−O bonds of optimum strength is important to yield high catalytic activity.[62,145] Additionally, Pt oxide formation plays a crucial role in electrocatalyst degradation due to the reductive dissolution under the ORR conditions of initially formed Pt^{2+} species.[146,147] The electrochemical oxidation of Pt NPs has been widely studied for single-crystal surfaces and NPs using in situ X-ray absorption and diffraction.[35,126,133,134] For example, the electrochemical oxidation of size-selected Pt NPs (∼1.2 nm) was investigated using in situ high-energy resolution fluorescence detection (HERFD) XANES recorded at the Pt L_3-edge (Figure 5k).[126] The oxidation was tracked by recording Pt L_3 XANES spectra during potential step experiments between ∼0 V and ∼1.2 V, and two distinct features attributed to metallic Pt and to Pt^{n+} species were considered. Peak fitting suggests that the Pt NPs are metallic up to ∼0.9 V, while OH_x coverage increases with the potential. Above 0.9 V, the Pt NPs oxidize to form PtO-like species concomitant with metallic Pt. Above 1.1 V the contribution of the metallic Pt feature decreases significantly, suggesting its transformation to PtO_x species. Comparing the experimental data to calculated XANES spectra led to the conclusion that at 1.2 V half of the Pt atoms are oxidized and can be best described as $Pt^{2+\delta}$ species. In a different study, the oxidation behavior of Pt NPs with a mean size of ∼2.6 nm was investigated using a combination of in situ XAFS at the Pt L_3 and XRD, and a special focus was placed on the structural response at potentials above 1.5 V.[133] Therein, only the upper two Pt layers of the NPs oxidize up to 1.5 V, leading to a lower structural coherence length of the Pt metal domains, as revealed from the broadening of the diffraction peaks. Above 1.5 V the anodic dissolution of Pt ions into the electrolyte was concluded from the decreasing diffraction peak intensity as well as edge height of the XANES spectra. These studies show how X-ray-based techniques can give insights into changes in the chemical state of NP electrocatalysts.

The evolution of the structure and chemical composition of O_2-plasma-pretreated micellar Au NPs was investigated via operando XAFS during 2-propanol electro-oxidation.[24] During electrochemical conditioning and 2-propanol oxidation, the XANES features typical of oxides present in the as-prepared samples as well as the Au−O typical peaks in the Fourier transform of the (FT-)EXAFS spectra disappeared, while the metallic Au−Au CNs increased. These findings also showed

DOI: 10.1021/acscatal.9b01831
ACS Catal. 2019, 9, 10020−10043

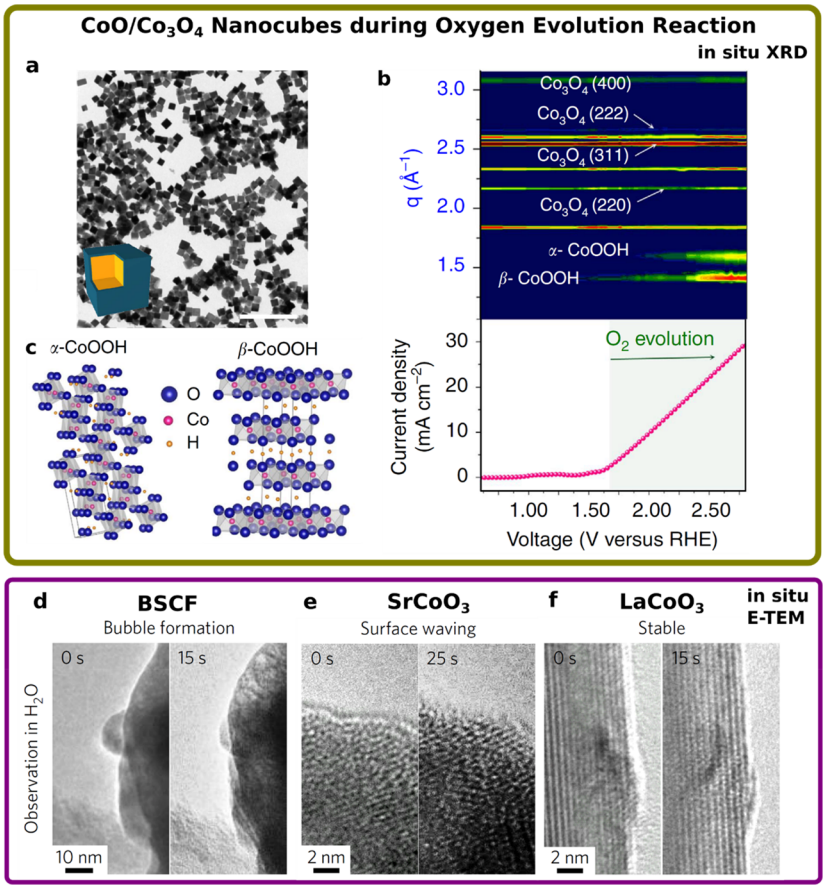

Figure 6. (a) TEM image of as-prepared CoO-covered Co_3O_4 nanocubes. The scale bar represents 200 nm. (b) In situ XRD pattern and cyclic voltammogram recorded from the nanocubes under OER conditions in alkaline electrolyte as well as (c) schematics of the CoOOH phases generating the adaption formed during OER. (d−f) In situ TEM images of $Ba_{0.5}Sr_{0.5}Co_{0.8}Fe_{0.2}O_{3-\delta}$ (BSCF), $SrCoO_{3-\delta}$ (SCO), and $LaCoO_3$ (LCO) NPs during electron beam induced oxygen evolution leading to bubble formation and structural oscillations for BSCF. (a)−(c) are reproduced from figures in ref 157. (d)−(f) are reproduced with permission from figures in refs 159. Copyright 2017 Springer-Nature.

that, despite the initial atomic oxygen exposure leading to the formation of Au^{3+} species, metallic Au is the active species for 2-propanol electro-oxidation to CO_2.

For the oxygen evolution reaction (OER), Ir-based as well as Co- and Ni-based materials are state of the art catalysts in acidic as well as in neutral and alkaline electrolytes, respectively, and they have been widely studied using in situ techniques.[25,130,131,148−158] In a recent study including in situ XAFS, the local atomic Co structure in nanostructured and NP electrocatalysts was found to unify under OER conditions.[155] For example, pyramidally shaped wurtzite-like CoO NPs oxidize during the OER toward a $CoO_x(OH)_y$ primarily containing octahedrally coordinated di-μ-oxo-bridged Co^{3+} ions. This oxidation process is accompanied by a significant roughening of the NP facets after the OER. The oxygen-evolving state is characterized by a contracted Co−O bond length. Furthermore, in situ XRD has been applied on CoO-covered Co_3O_4 nanocubes under technologically relevant alkaline OER conditions and a reversible formation of a crystalline CoOOH adaption layer was unraveled, Figure 6a−c.[157] These results are in agreement with findings on nanoporous Co_3O_4 films showing a reversible decrease of the Co_3O_4 nanocrystallite coherence length during the OER.[154] These and other works applying in situ Co K-edge XANES spectroscopy suggest changes in the charge of the Co ions and the presence of $Co^{3+\delta}$ during the OER.[130,131,154−156,158]

Similarly, an in situ XAFS investigation on Ir-based NPs suggests that Ir ions oxidize during the OER to an oxidation state formally higher than 4+.[148,152] Nevertheless, the presence of reactive oxygen species (O^-) has also been reported for Ir-based electrocatalysts under OER conditions by combining in situ O K-edge XANES spectra and DFT calculations.[150,151] Similar changes were revealed in Co-based catalysts by in situ XPS based on the dip-pull method.[160] Thus, the location of oxidation equivalents on metal oxide NPs which are necessary for water oxidation and the OER is still under debate. The latter highlights the necessity of further in situ studies on model NP catalysts under OER conditions.

All of these findings suggest that the catalytically relevant structure of the OER catalysts is not well described by idealized single-crystal surfaces but rather has a disordered and/or dynamic near surface. This is even further supported by findings on the highly OER-active $Ba_{0.5}Sr_{0.5}Co_{0.8}Fe_{0.2}O_{3-\delta}$ (BSCF) NPs with a diameter of ∼150 nm investigated using E-TEM under NAP conditions to mimic the OER (Figure 6d−f).[159] Although using water vapor as reactant and studying e-beam induced reactions do not represent the "real" catalytic conditions, the BSCF NPs are prone to structural oscillations on the nanoscale during e-beam-induced oxygen evolution, as shown in Figure 6d. Gas bubble formation could be linked to the dynamics of the lattice in the near surface of the NP via electron energy loss spectroscopy (EELS). Significantly

DOI: 10.1021/acscatal.9b01831
ACS Catal. 2019, 9, 10020−10043

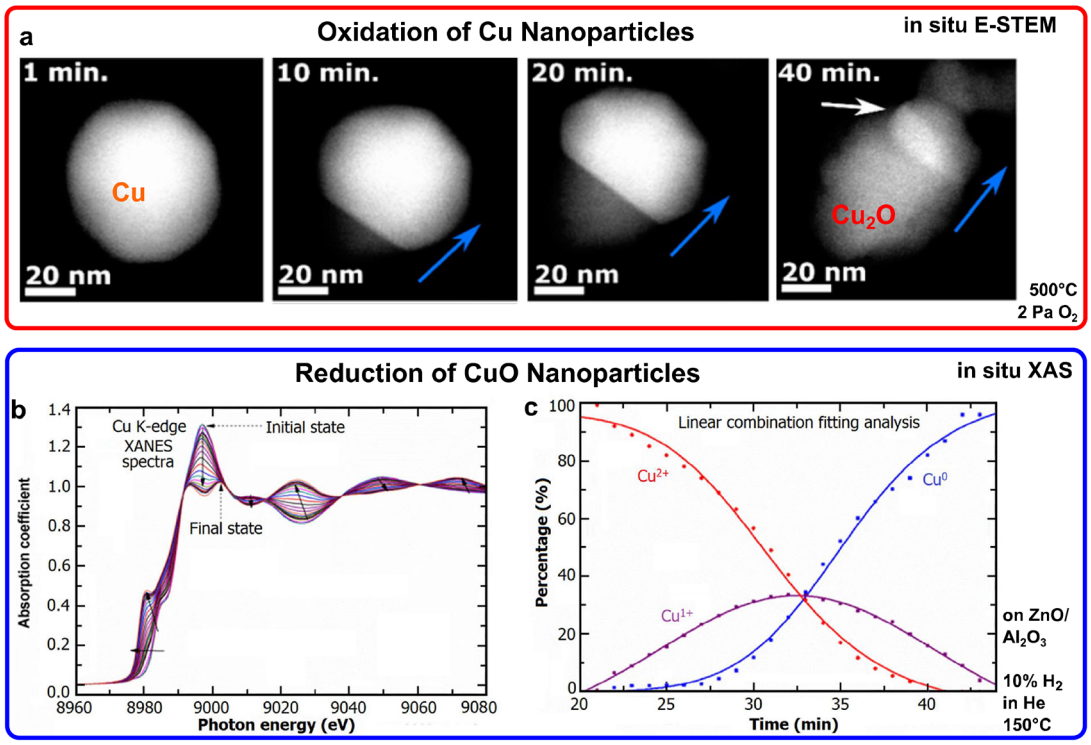

Figure 7. (a) In situ E-STEM images recorded during gas-phase oxidation of an individual Cu NP to Cu_2O. In situ time-resolved XANES of CuO NPs recorded at the Cu K-edge during gas-phase reduction in 10%H_2/He at 150 °C (b) and the corresponding linear combination analysis (c). CuO NPs are present after calcination of a Cu/ZnO/Al_2O_3 catalyst for methanol synthesis. (a) and (b)−(c) are reproduced with permission from figures in refs 177 and 180, respectively. Copyright 2017 American Chemical Society and 2016 Shanghai Institute of Applied Physics, Chinese Academy of Sciences, Chinese Nuclear Society, Science Press China and Springer Science+Business Media Singapore, respectively.

suppressed or absent oscillations were found for other less OER-active Co-based perovskites such as $SrCoO_{3-\delta}$, shown in Figure 6e, and $LaCoO_3$, shown in Figure 6f.

All these in situ works on 3d transition-metal-based OER catalysts revealed that the (near) surface of these nanocatalysts is not identical with the as-prepared single crystal state but rather is disordered during water oxidation and oxygen evolution. Structural flexibility is either a necessity or the disorder a result of the reaction.

3.1.2. 3d Transition-Metal-Based Nanoparticle Catalysts under Reducing Reaction Conditions. In addition to noble-metal electrocatalysts, 3d transition-metal-based NPs and nanocatalysts have received strong attention due to their abundance and catalytic activity. Two material classes based on 3d TM NPs excel by their relevance for industrial processes based on thermal catalysis: Cu NPs supported on ZnO for methanol synthesis during CO_2 hydrogenation[86,102,161,162] and supported Co NPs for Fischer−Tropsch synthesis (FTS) of hydrocarbons.[163−176] Furthermore, increasing efforts have been invested in the investigation of Cu-based NPs for the CO_2RR to efficiently produce multicarbon products such as ethanol and ethylene.[53−56] In situ studies have been applied to investigate the chemical state and redox chemistry of Cu NPs under various conditions.[162,177−182] For Cu-based NPs, particular attention has to be paid to oxide formation under ambient conditions.[95] Thus, the transition from ambient to reaction conditions involves a chemical or electrochemical reduction: e.g., a reductive pretreatment is used as part of the catalyst activation protocol for high-pressure CO_2 hydrogenation.[86] When this is taken into account, the redox chemistry of Cu-based NPs was investigated using E-STEM, showing that Cu NPs oxidize and the formed Cu_2O NPs reduce in a very similar fashion, although with significantly different kinetics.[177] The Cu NP oxidation starts at a single point and proceeds with an oxidation front along the NPs, as shown in Figure 7a. During Cu_2O reduction under H_2-containing NAP conditions, oxygen vacancies migrate into the bulk of the NP and accumulate at the Cu_2O/Cu interface. A correlation between the accumulation of O vacancies and a lattice contraction leading to a collapse of the crystal lattice above a vacancy concentration of 50% was identified.[178] The redox chemistry of chemically prepared Cu_2O NCs and their light-induced structural transformation were investigated to illuminate the degradation pathway of this photocatalyst.[179] Therein, the photoreduction of Cu_2O to metallic Cu under UV light irradiation and in the presence of 5 mbar of water vapor led to an ∼25% decrease in the NC size. Interestingly, a gradual transition was identified, as both phases coexist in the same NC within the reduction. In the case of industrial CO_2 hydrogenation catalysts, a similar gradual reduction of CuO NPs supported on ZnO/Al_2O_3 was revealed using in situ XAFS.[180] The calcined NPs can be reduced to metallic Cu in 10% H_2/He at 150 °C within less than 30 min, Figure 7b,c. The reduction was reported to proceed via Cu(I) formation with an interstitial O in the Cu lattice forming a substoichiometric Cu oxide.

A similar reaction process was determined for Cu NPs supported on or embedded in $ZnAl_2O_4$, as revealed by a combined TPR and in situ XANES spectra recorded at the Cu L_3-edge.[162] In a reactant gas mixture for methanol synthesis, the reduction process also proceeds via a lower fraction of intermediate Cu^+ species.[181] Furthermore, the reduction

DOI: 10.1021/acscatal.9b01831
ACS Catal. 2019, 9, 10020−10043

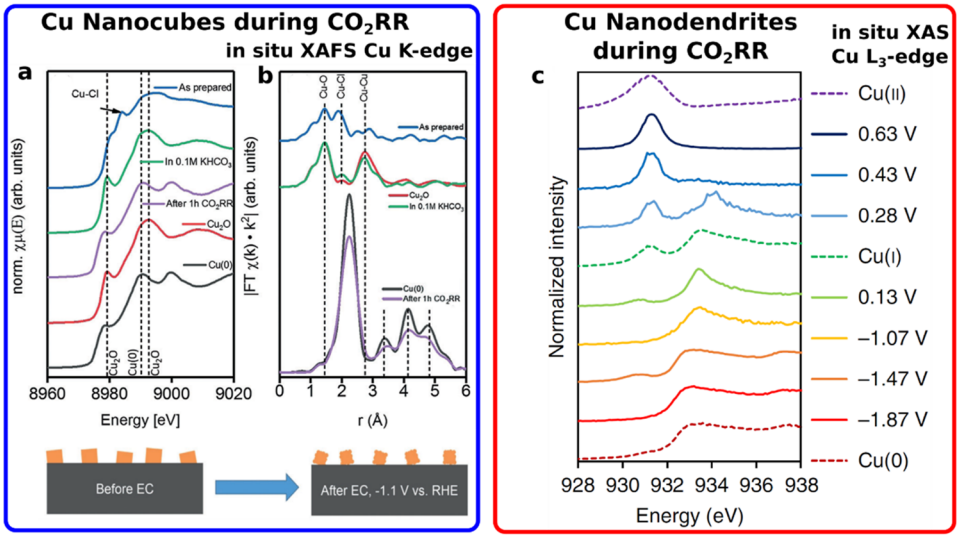

Figure 8. (a, b) Operando Cu K-edge XANES and FT-EXAFS spectra recorded for electrochemically prepared Cu nanocubes in the as-prepared state, after immersion in the electrolyte, and during CO_2RR operation, respectively. (c) XANES recorded at the Cu L_3-edge of electrochemically deposited Cu nanodendrites are shown for selected electrode potentials covering the CO_2RR region. All studies were conducted in a CO_2-saturated 0.1 M $KHCO_3$ electrolyte. (a)−(b) and (c) are reproduced and adapted with permission from figures in refs 39 and 193, respectively. Copyright 2018 Wiley-VCH and 2018 Springer-Nature, respectively.

process was found to be size-dependent for Cu clusters supported on hydroxylated Al_2O_3, as studied with in situ grazing-incidence XANES, and the reduction temperature was found to decrease in the order $Cu_3 > Cu_4 > Cu_{20}$.[182] Notably, the onset for methanol formation follows the reduction temperature.

Under the actual CO_2 hydrogenation conditions, the Cu and Zn oxidation states and local atomic structures did not change significantly.[180] These findings are in agreement with the structural integrity of the Cu NPs as revealed in an in situ diffraction study.[104]

The second highly relevant heterogeneous reaction where chemical state changes in the NPs have been reported is the Fischer−Tropsch synthesis. Typical FTS catalysts consist of Co NPs supported on Al_2O_3, SiO_2, carbon, and TiO_2.[183] In situ methods, mostly combining XRD and XAFS, have been used to study aspects related to the catalyst activation, the active catalyst state, and deactivation pathways for the Co NPs.[163−176] For example, the reduction of Co oxide NP precatalysts was studied during a H_2-based activation procedure at ∼400 °C[163−167] and full conversion of Co_3O_4 to metallic Co was reached after several hours, going through a CoO intermediate which is present between 200 and 350 °C.[166−168] The activated Co-based Fischer−Tropsch catalyst consisted of both hexagonal-close-packed (hcp) metallic Co NPs with a size of ∼2.5 nm and face-centered-cubic (fcc) Co NP swith a size of 20 nm present as primary and secondary phases, respectively.[168] The coexistence of Co in fcc and hcp phases has also been reported in other in situ XRD and E-TEM studies.[166,169] Under the reaction conditions, the Co NPs were found to remain in the metallic state and resist sintering within the first 10 days on stream investigated.[164,165,168,172] Co_2C formation was found during high-pressure FTS and under a pure CO atmosphere accompanied by a decreasing fraction of fcc Co, while the fraction of hcp Co remained constant.[168,171,173] As Co_2C is inactive for FTS, its formation is considered to be part of the degradation pathway of Co NP FTS catalysts. This is in contrast to the case of Fe-based FTS catalysts, in which Fe_2C is found to exhibit high catalytic activity.[184] Thus, in situ investigations on Co-based NP catalysts for FTS provided valuable insights on the reduction mechanism of Co oxides and on the structural integrity of the NPs under reaction conditions.

In the CO_2RR, the catalyst structure and morphology are decisive for the catalytic activity and selectivity, as small and/or defective NPs have been found to favor the HER.[56] The presence of subsurface oxygen or substoichiometric Cu oxides under the reaction conditions is under debate, but has been suggested to lead to high ethylene/ethanol yields.[185] Therefore, it is highly important to identify the chemical state, the structure, and the catalyst morphology under CO_2RR conditions. For this purpose, CO_2RR electrocatalysts have been investigated using a variety of in situ and operando techniques, such as Raman spectroscopy[7,125,186−190] and XPS[191] as well as XAFS at the Cu L_3- and K-edges.[39,125,192−195] Fewer in situ/operando studies on NP catalysts are available for the electrochemical CO_2RR in comparison to long-studied reactions such as methanol and Fischer−Tropsch synthesis. Therefore, in the following, we cover the chemical state changes of NP and nanostructured Cu-based electrocatalysts under CO_2RR conditions. In a recent study, the evolution of the chemical state and local atomic structure was investigated for electrochemically prepared Cu-based nanocubes (NCs) supported on C during CO_2RR.[39] In situ XAFS and quasi in situ XPS showed that their primary constituents in the as-prepared state are Cu_2O and Cu−Cl species in the bulk and at the surface. As described previously, immersing the NCs in the electrolyte not only significantly changed the morphology but also removed the Cu−Cl species. During the CO_2RR, the NCs supported on C are completely reduced to metallic Cu (Figure 8a), which is in agreement with other Cu-based NCs studied.[194] In contrast, those NCs grown on a Cu foil still show Cu_2O surface species by quasi in situ XPS after 1 h of the CO_2RR.[39,196] The latter finding is in agreement with results for plasma-treated Cu surfaces during the CO_2RR, for which the Cu oxide domains partially remain,

DOI: 10.1021/acscatal.9b01831
ACS Catal. 2019, 9, 10020−10043

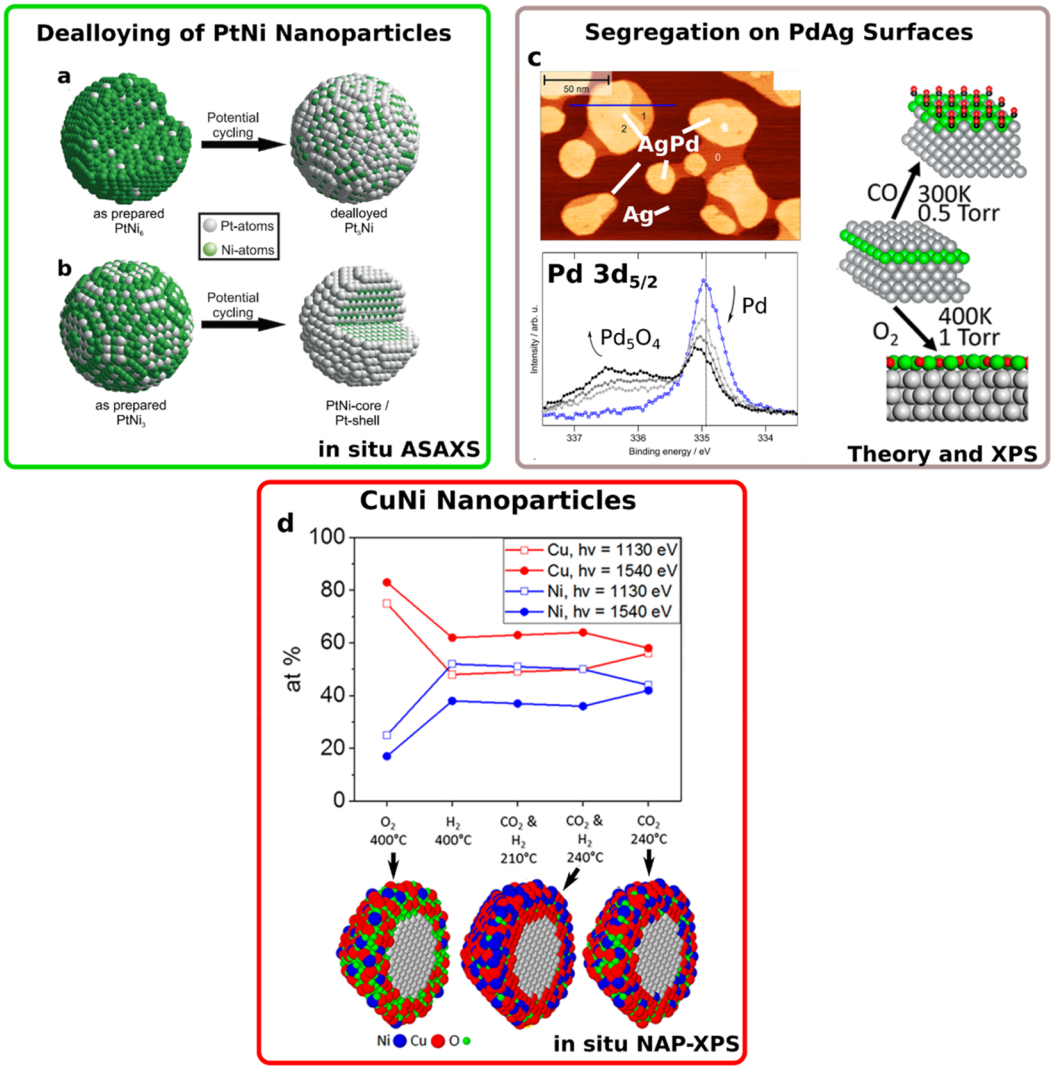

Figure 9. (a, b) Models of the structural evolution of PtNi alloy NPs during electrochemical dealloying procedures. The electrochemical dealloying was applied to generate core−shell NPs as extracted from in situ anomalous SAXS and pair-distribution function analysis. (c) Segregation of Pd in PdAg surface alloys at elevated temperatures under CO- and/or O_2-containing atmospheres as studied with STM, XPS and DFT calculations. (d) Near-surface compositional changes of size-selected CuNi NPs as extracted from NAP-XPS under O_2, H_2, CO_2, and CO_2 + H_2 containing atmospheres. (a)−(b), (c), and (d) are reproduced and adapted with permission from figures in refs 207, 209, and 210, respectively. Copyright 2013, 2019, and 2018 American Chemical Society, respectively.

as probed by operando EXAFS and corroborated by ex situ STEM-EELS.[195] For longer reaction times, no conclusive statement could be made on the basis of the operando XAFS data, since the bulk metallic signal dominated and this method is not sensitive to very thin surface oxide layers, even in the grazing geometry used in this study. Interestingly, online product analysis shows that the Faradaic efficiency and thus the selectivity toward ethylene benefits from the oxidative plasma treatment, while the yield of methane almost vanishes. This work shows that the catalytic function can be tuned by applying a plasma activation pretreatment leading to a modified catalyst morphology and chemical state. The presence of subsurface or adventitious oxygen was identified in oxide-derived Cu electrocatalysts by using in situ NAP-XPS based on the dip-pull method.[191] Even under reductive CO_2RR conditions, the adventitious oxygen signal in the O 1s XP spectra remained, whereas no spectroscopic fingerprint of Cu_2O and CuO species was found. Thus, this indicated the absence of distinct CuO_x phases in the reduced state and the absence of any Cu^{2+} species was confirmed by Cu 2p XP spectra. Generally, we note that the approach of utilizing an electrochemical flow cell with a graphene electron-transparent window for in situ electrochemical X-ray photoelectron spectroscopy should be favored, because it allows stationary, realistic catalytic conditions by minimizing mass transport limitations and radical or product accumulation via constant electrolyte exchange. The presence of Cu^+ species under CO_2RR conditions was furthermore shown using in situ Cu L_3-edge XANES spectra (Figure 7b).[193] Therein, a gradual transition from Cu^{2+} to Cu^0 with decreasing potential under quasi-stationary conditions was revealed, but it was shown that complete electrochemical reduction during the CO_2RR takes 1 h.

Another study highlighted possible deactivation processes hampering the electrochemical reduction of CuO in the presence of carbonate ions.[192] The formation of Cu carbonates can passivate CuO electrocatalysts, as shown by XANES at the Cu L_3-edge, leading to negligible catalytic activity. In the case

DOI: 10.1021/acscatal.9b01831
ACS Catal. 2019, 9, 10020−10043

of Cu_2O and metallic Cu electrocatalysts, the deactivation process was not seen and in both cases metallic Cu was found to be the dominant species under CO_2RR conditions. Combining the structural and morphological changes with the formed reaction products shows the detrimental effect on C_2-C_3 selectivity of having small Cu nanocatalysts or those completely free of oxygen. These studies likewise show the importance of having combined morphological, structural, and chemical state insights into the catalyst properties under reaction conditions by using various in situ techniques to understand the catalyst function and its relation to the structure and morphology. However, the variety of partially contrary experimental findings on the presence of Cu^+ or substoichiometric Cu oxides under CO_2RR reaction conditions on differently synthesized samples, as well as insufficient theoretical descriptions, has prevented to date the formulation of unambiguous statements on their mechanistic role. The latter discrepancies also highlight the need of using a variety of complementary but synergetic techniques operating under reaction conditions for an understanding of electrocatalytic processes, since the probe depth and sensitivity to the chemical state or the presence of amorphous versus crystalline species that might be extracted from the distinct methods will be different.

3.2. (Near-)Surface Compositional Changes and Segregation under Reaction Conditions. The activity of NP catalysts can strongly depend on their composition not only in the near surface but also in the bulk. For example, it has been shown that core−shell NPs exhibit a significantly higher catalytic activity as fuel cell catalysts.[29,197−202] Therein, the lattice strain in the NP shell induced by compositional differences to the bulk varies the electronic structure and d-band center. The metal d-band center directly influences the bond strength of adsorbates and reaction intermediates, and thus tuning the electronic structure of the surface can lead to improved catalytic activity.[203−205]

Electrochemical potential cycling is often applied as an accelerated stress test (AST) for fuel cell catalysts, but it can induce substantial changes in the near-surface composition of Pt-based alloy NPs and the formation of core−shell NPs.[204,206−208] For example, in situ anomalous SAXS and pair distribution function analysis was applied to study the segregation and atomic ordering in PtNi NPs under electrochemical potential cycling (Figure 9a,b).[207] The electrochemical potential cycling was applied as a dealloying procedure for activation. In this study, the formation of a Ni-free shell was tracked and the transformation of the bulk PtNi solid solution into an ordered PtNi alloy revealed. In the case of octahedral Au NPs with a Pd shell, electrochemical potential cycling diminishes the core−shell structure and leads to a more homogeneous distribution of elements within the entire NP.[204]

In the case of spherical PtCo NPs under gas-phase oxidizing and reducing conditions in an E-TEM, Co surface segregation and the formation of CoO islands was revealed. In the intermediate step, strained CoO films formed at the NP surface. Under reductive conditions, the Co atoms migrate into the bulk of the NP, leading to a pure Pt termination. Adsorbate-induced segregation was theoretically studied using DFT for an Au/Pd bimetallic surface in the case of CO.[211] In contrast to the bare Au surface on Pd, Pd migration to the surface and clustering were stronger in the presence of adsorbed CO.

The presence of Au vacancies on the surface significantly facilitate the Au−Pd swapping process, and the larger Pd NPs bind O_2 rather than CO. In the case of Pd−Ag alloys, the segregation process has been investigated by means of DFT during O_2, CO, and C_2H_2 adsorption.[209,212] Therein, it was revealed that acetylene adsorption reorders the Pd−Ag surface under simulated reaction conditions relevant for catalytic acetylene selective hydrogenation. In a combined experimental surface science and theoretical work, it was shown that on Ag(111) nanoislands of an AgPd alloy are formed and that they are Ag-terminated under UHV conditions (Figure 9c).[209] At elevated temperatures under CO conditions, Pd irreversibly migrates to the surface accompanied by an energetic stabilization of the Pd−CO bond. A similar process was identified under O_2-containing conditions. Thus, this atom migration process is assigned to be the catalytic activation process. This study nicely shows how, by a combination of experimental (surface science) techniques and theoretical calculations, atomic segregation processes can be revealed and explained.

Segregation is also attributed to cause the deactivation of nanoporous Au due to residual Ag atoms. During nanocoarsening under CO oxidation conditions, the residual Ag atoms in these structures were found to rearrange and segregate to the surface, forming AgO_x islands.[64] Ag surface segregation is enhanced by an ozone-based treatment of the nanoporous Au, and the chemical state of the oxide nature of the Ag-containing islands was identified using EELS.[68] These domains were discussed to provide O_2 dissociation sites for CO oxidation, and distinct O species were described after the activation procedure on the basis of NAP-XPS data.

The segregation of bimetallic NPs under gas-phase reaction conditions was investigated for CuNi NPs using NAP-XPS under simulated CO_2 hydrogenation conditions (Figure 9d).[210,213] Therein, Ni surface segregation was identified in the case of an O_2-containing atmosphere and is even stronger in a $CO_2 + H_2$ reaction mixture after reductive pretreatment. The presence of H-containing adsorbates as well as CO was attributed to cause the Ni segregation under simulated reaction conditions. In contrast, Cu surface segregation was revealed in a reaction mixture containing $CO_2 + CO + H_2$, and DFT calculations suggested that CH_3O, a stable reaction intermediate, could induce a reverse segregation energy for Cu and Ni under reaction conditions.[213]

Here, we note that in situ investigations on the compositional changes and metal segregation under reaction conditions are especially important because the composition is prone to change even under ambient conditions due to the differences in the oxophilicity of the elements.

4. OUTLOOK

The presented in situ and operando studies focusing on NP transformations under gas-phase thermal and electrochemical catalytic conditions exemplify the insights that can be achieved with respect to the NP morphology, structure, chemical state, and composition using today's state of the art experimental tools. However, a more comprehensive picture of a working catalyst is still necessary for the quest of the active site as well as to go beyond the active site towards the entire catalytic system, extracting design principles for more active and/or stable catalysts. Therefore, improved experimental studies with respect to their methodology and the performance of the applied methods are still needed.

DOI: 10.1021/acscatal.9b01831
ACS Catal. 2019, 9, 10020−10043

First, we showed that the combination of operando techniques probing different properties of the catalysts such as the structure/morphology and the adsorbates as well as the reaction products in combined experiments yields a comprehensive picture of the active catalyst. However, these insights have been mainly limited to the investigation of NPs under gas-phase thermal reaction conditions. In the years to come, additional effort should be made in order to have such combined in situ/operando methods more extensively applied to the study of electrochemical catalytic processes. Combining local microscopy methods revealing the NP morphology with statistical methods such as XAFS or XRD showing the catalyst structure would significantly contribute to gaining more in-depth insight into the heterogeneity of NP properties in the working catalysts.[43]

Furthermore, we note that the simultaneous detection of reaction products and the determination of rates during in situ experiments, transforming them into operando investigations, is essential to identify function−property relationships. However, in the field of electrocatalysis this approach has not been established to the same extent as it has in thermal catalysis, and often the catalyst selectivity is analyzed in separate laboratory-based experiments. Here, the online analysis of gaseous products using gas chromatography and/or parallel liquid product analysis using high-pressure liquid chromatography or mass spectrometry should be combined with operando structural and vibrational spectroscopic methods such as XRD, XAFS, IR, or Raman spectroscopy for the concomitant analysis of adsorbates, reaction intermediates, and structural/chemical modifications of the working catalyst.[7] In reactions such as the electrochemical water splitting or oxygen evolution, the number of possible reaction products is strongly limited. Nevertheless, the simultaneous detection of dissolved metal ions using inductively coupled plasma mass spectrometry (ICP-MS) would be ideal to gain further insight into the NP catalyst response to varying redox reaction conditions and its deactivation pathways via metal dissolution or NP detachment.[214] The presence of a liquid medium in electrochemistry significantly enhances the rate of removal of unstable intermediates from the NP surface, which emphasizes the need for additional operando stability studies to monitor the evolution of the NP loading on the support.

Additionally, operando experiments on NP catalysts based on X-rays are mainly conducted at synchrotron facilities, which limits the available experimental time and hampers the researchers' ability to conduct long-term stability studies on technologically relevant time scales. As noted above, these studies are essential to study the evolution of NP catalyst properties over the (whole) catalyst lifetime. This is especially important for highly oxygen sensitive catalysts such as metal NPs, which cannot be taken out of the reaction conditions prior to the end of the catalyst lifetime. Therefore, the development of additional suitable laboratory-based X-ray setups for operando catalyst characterization is primordial in order to open up the possibility of performing long-term durability experiments in house, extending the characterization time scales from a few days to weeks or months. This has already been implemented in operando XRD studies of NP catalysts under FTS conditions.[168] It is expected that laboratory XAFS setups and the implementation of suitable operando cells will speed up this needed development.[215,216]

Generally, it is also clear that conventional in situ/operando investigations are limited with respect to the identification of the catalytically active site on NPs. Usually, the long-lived state in the catalytic cycle is probed as a majority species on the active sites, which is by definition the state preceding the rate-determining step. The actual active states at which the crucial reaction step(s) proceed are most likely minority or trace species with a significantly shorter lifetime. Furthermore, the heterogeneity of most catalysts impedes the clarity of the obtained experimental observations. To fundamentally understand chemical reactions, more studies focusing on size- and shape-controlled NPs should be conducted so that activity-/selectivity-determining properties can be more easily isolated. In this case distinct trends in NP properties such as the chemical state of surface and bulk atoms could be extracted from a series of measurements on differently sized NPs. Time-resolved in situ methods such as pump−probe experiments will allow the tracking of adsorbates, (electronic) structure, and composition changes during (electro)chemical reactions on millisecond to femtosecond time scales, leading to an improved understanding of active and spectator sites on a NP surface or its support. Some works have already given important insights in this field,[217−219] but many of these methods need to be adapted to investigate a wider variety of NP catalysts under different reaction conditions. In this respect, ongoing advances in the development of experimental setups at X-ray free electron lasers and synchrotron facilities are expected to accelerate the fundamental understanding of catalytic processes at the atomic scale.

5. CONCLUSION

In this work, we have presented a variety of in situ and operando studies revealing morphological, structural, and chemical state transformations of nanosized heterogeneous catalysts. The presented works mainly cover redox transitions of the nanoparticles under H_2- and O_2-containing atmospheres as well as the active state under gas-phase and electrochemical reaction conditions that are important within the framework of chemical energy conversion such as CO_2 hydrogenation and electroreduction as well as the oxygen evolution reaction. We presented various X-ray-based in situ/operando studies which revealed the transformation of NP catalysts under thermal and electrochemical reaction conditions with respect to crystallinity, chemical state, and local atomic structure. These studies provide a representative picture of the catalytically active state by probing a statistically relevant number of catalyst nanoparticles. Nevertheless, these techniques are not suitable to detect minor or trace species that can be of greater importance for the catalysis than the majority of spectator species, e.g. as potentially the Cu^+ species during CO_2RR. Deep insight into the atomic processes on the surface of selected NPs could be obtained from environmental (S)TEM studies. Nevertheless, in these studies, the low reactant concentration hampered a comparison to realistic reaction conditions and it seems as if obtainable lateral resolution and reactant concentration, in the gas phase as well as the liquid phase, has to be compromised. In this respect, verifying the findings from environmental electron microscopy with either parallel statistical in situ/operando insights or ex situ property−function correlations leads to a more comprehensive picture of the catalyst under reaction conditions. We think that in situ/operando studies have already given important insights in catalysis research and their further methodical progress, especially with respect to investigations of the catalyst dynamics, will allow researchers to

DOI: 10.1021/acscatal.9b01831
ACS Catal. 2019, 9, 10020−10043

increase their fundamental knowledge of the catalytically active state of nanoparticles.

AUTHOR INFORMATION

Corresponding Author

*E-mail for B.R.C.: roldan@fhi-berlin.mpg.de.

ORCID

Beatriz Roldan Cuenya: 0000-0002-8025-307X

Author Contributions

The manuscript was written through contributions of all authors. All authors have given approval to the final version of the manuscript.

Notes

The authors declare no competing financial interest.

ACKNOWLEDGMENTS

We are grateful for the financial support of the Deutsche Forschungsgemeinschaft (DFG, German Research Foundation)—project no. 405034883—TRR 247, and project no. 327886311—SFB 1316, as well as the Germany Excellence Strategy—EXC 2008/1 (UniSysCat)—390540038. The financial support of the European Research Council under grant ERC-OPERANDOCAT (ERC-725915) is also greatly appreciated.

REFERENCES

(1) Haber, F.; Le Rossignol, R. Über Die Technische Darstellung Von Ammoniak Aus Den Elementen. *Zeitschrift für Elektrochemie und angewandte physikalische Chemie* **1913**, *19*, 53−72.

(2) Smil, V. *Enriching the Earth - Fritz Haber, Carl Bosch, and the Transformation of World Food Production*; MIT Press: 2004.

(3) Goodman, D. W. Catalysis: From Single Crystals to the "Real World. *Surf. Sci.* **1994**, *299*−*300*, 837−848.

(4) Liu, L.; Corma, A. Metal Catalysts for Heterogeneous Catalysis: From Single Atoms to Nanoclusters and Nanoparticles. *Chem. Rev.* **2018**, *118*, 4981−5079.

(5) Kalz, K. F.; Kraehnert, R.; Dvoyashkin, M.; Dittmeyer, R.; Gläser, R.; Krewer, U.; Reuter, K.; Grunwaldt, J.-D. Future Challenges in Heterogeneous Catalysis: Understanding Catalysts under Dynamic Reaction Conditions. *ChemCatChem* **2017**, *9*, 17−29.

(6) Gao, X.; Bañares, M. A.; Wachs, I. E. Ethane and N-Butane Oxidation over Supported Vanadium Oxide Catalysts: An in Situ UV−Visible Diffuse Reflectance Spectroscopic Investigation. *J. Catal.* **1999**, *188*, 325−331.

(7) Bañares, M. A.; Guerrero-Pérez, M. O.; Fierro, J. L. G.; Cortez, G. G. Raman Spectroscopy During Catalytic Operations with on-Line Activity Measurement (Operando Spectroscopy): A Method for Understanding the Active Centres of Cations Supported on Porous Materials. *J. Mater. Chem.* **2002**, *12*, 3337−3342.

(8) Campbell, C. T. Bimetallic Surface Chemistry. *Annu. Rev. Phys. Chem.* **1990**, *41*, 775−837.

(9) Campbell, C. T. The Energetics of Supported Metal Nanoparticles: Relationships to Sintering Rates and Catalytic Activity. *Acc. Chem. Res.* **2013**, *46*, 1712−1719.

(10) Hansen, P. L.; Wagner, J. B.; Helveg, S.; Rostrup-Nielsen, J. R.; Clausen, B. S.; Topsøe, H. Atom-Resolved Imaging of Dynamic Shape Changes in Supported Copper Nanocrystals. *Science* **2002**, *295*, 2053.

(11) Benavidez, A. D.; Kovarik, L.; Genc, A.; Agrawal, N.; Larsson, E. M.; Hansen, T. W.; Karim, A. M.; Datye, A. K. Environmental Transmission Electron Microscopy Study of the Origins of Anomalous Particle Size Distributions in Supported Metal Catalysts. *ACS Catal.* **2012**, *2*, 2349−2356.

(12) Behafarid, F.; Pandey, S.; Diaz, R. E.; Stach, E. A.; Cuenya, B. R. An in Situ Transmission Electron Microscopy Study of Sintering and Redispersion Phenomena over Size-Selected Metal Nanoparticles: Environmental Effects. *Phys. Chem. Chem. Phys.* **2014**, *16*, 18176−84.

(13) Behafarid, F.; Roldan Cuenya, B. Towards the Understanding of Sintering Phenomena at the Nanoscale: Geometric and Environmental Effects. *Top. Catal.* **2013**, *56*, 1542−1559.

(14) DeLaRiva, A. T.; Hansen, T. W.; Challa, S. R.; Datye, A. K. In Situ Transmission Electron Microscopy of Catalyst Sintering. *J. Catal.* **2013**, *308*, 291−305.

(15) Luo, L.; Engelhard, M. H.; Shao, Y.; Wang, C. Revealing the Dynamics of Platinum Nanoparticle Catalysts on Carbon in Oxygen and Water Using Environmental Tem. *ACS Catal.* **2017**, *7*, 7658−7664.

(16) Zhu, G. Z.; Prabhudev, S.; Yang, J.; Gabardo, C. M.; Botton, G. A.; Soleymani, L. In Situ Liquid Cell Tem Study of Morphological Evolution and Degradation of Pt-Fe Nanocatalysts During Potential Cycling. *J. Phys. Chem. C* **2014**, *118*, 22111−22119.

(17) Hodnik, N.; Dehm, G.; Mayrhofer, K. J. Importance and Challenges of Electrochemical in Situ Liquid Cell Electron Microscopy for Energy Conversion Research. *Acc. Chem. Res.* **2016**, *49*, 2015−22.

(18) Liu, L.; Zakharov, D. N.; Arenal, R.; Concepcion, P.; Stach, E. A.; Corma, A. Evolution and Stabilization of Subnanometric Metal Species in Confined Space by in Situ Tem. *Nat. Commun.* **2018**, *9*, 574.

(19) Tao, F. F.; Crozier, P. A. Atomic-Scale Observations of Catalyst Structures under Reaction Conditions and During Catalysis. *Chem. Rev.* **2016**, *116*, 3487−539.

(20) Yoshida, H.; Kuwauchi, Y.; Jinschek, J. R.; Sun, K.; Tanaka, S.; Kohyama, M.; Shimada, S.; Haruta, M.; Takeda, S. Visualizing Gas Molecules Interacting with Supported Nanoparticulate Catalysts at Reaction Conditions. *Science* **2012**, *335*, 317.

(21) Lira, E.; Merte, L. R.; Behafarid, F.; Ono, L. K.; Zhang, L.; Roldan Cuenya, B. Role and Evolution of Nanoparticle Structure and Chemical State During the Oxidation of No over Size- and Shape-Controlled Pt/Γ-Al_2O_3 Catalysts under Operando Conditions. *ACS Catal.* **2014**, *4*, 1875−1884.

(22) Newton, M. A.; Belver-Coldeira, C.; Martinez-Arias, A.; Fernandez-Garcia, M. Dynamic in Situ Observation of Rapid Size and Shape Change of Supported Pd Nanoparticles During Co/No Cycling. *Nat. Mater.* **2007**, *6*, 528−32.

(23) Paredis, K.; Ono, L. K.; Behafarid, F.; Zhang, Z.; Yang, J. C.; Frenkel, A. I.; Cuenya, B. R. Evolution of the Structure and Chemical State of Pd Nanoparticles During the in Situ Catalytic Reduction of No with H2. *J. Am. Chem. Soc.* **2011**, *133*, 13455−64.

(24) Choi, Y.; Sinev, I.; Mistry, H.; Zegkinoglou, I.; Roldan Cuenya, B. Probing the Dynamic Structure and Chemical State of Au Nanocatalysts During the Electrochemical Oxidation of 2-Propanol. *ACS Catal.* **2016**, *6*, 3396−3403.

(25) Pedersen, A. F.; Escudero-Escribano, M.; Sebok, B.; Bodin, A.; Paoli, E.; Frydendal, R.; Friebel, D.; Stephens, I. E. L.; Rossmeisl, J.; Chorkendorff, I.; Nilsson, A. Operando XAS Study of the Surface Oxidation State on a Monolayer IrO_x on RuO_x and Ru Oxide Based 1475 Nanoparticles for Oxygen Evolution in Acidic Media. *J. Phys. Chem. B* **2018**, *122*, 878−887.

(26) Hejral, U.; Muller, P.; Balmes, O.; Pontoni, D.; Stierle, A. Tracking the Shape-Dependent Sintering of Platinum-Rhodium Model Catalysts under Operando Conditions. *Nat. Commun.* **2016**, *7*, 10964.

(27) Schmies, H.; Bergmann, A.; Drnec, J.; Wang, G. X.; Teschner, D.; Kuhl, S.; Sandbeck, D. J. S.; Cherevko, S.; Gocyla, M.; Shviro, M.; Heggen, M.; Ramani, V.; Dunin-Borkowski, R. E.; Mayrhofer, K. J. J.; Strasser, P. Unravelling Degradation Pathways of Oxide-Supported Pt Fuel Cell Nanocatalysts under in Situ Operating Conditions. *Adv. Energy Mater.* **2018**, *8*, 1701663.

(28) Hornberger, E.; Bergmann, A.; Schmies, H.; Kuhl, S.; Wang, G. X.; Drnec, J.; Sandbeck, D. J. S.; Ramani, V.; Cherevko, S.; Mayrhofer, K. J. J.; Strasser, P. In Situ Stability Studies of Platinum Nanoparticles Supported on Ruthenium-Titanium Mixed Oxide (RTO) for Fuel Cell Cathodes. *ACS Catal.* **2018**, *8*, 9675−9683.

DOI: 10.1021/acscatal.9b01831
ACS Catal. 2019, 9, 10020−10043

(29) Escudero-Escribano, M.; Pedersen, A. F.; Ulrikkeholm, E. T.; Jensen, K. D.; Hansen, M. H.; Rossmeisl, J.; Stephens, I. E. L.; Chorkendorff, I. Active-Phase Formation and Stability of Gd/Pt(111) Electrocatalysts for Oxygen Reduction: An in Situ Grazing Incidence X-Ray Diffraction Study. *Chem. - Eur. J.* **2018**, *24*, 12280−12290.
(30) Lee, S.; Lee, S.; Kumbhalkar, M. D.; Wiaderek, K. M.; Dumesic, J.; Winans, R. E. Effect of Particle Size Upon Pt/SiO_2 Catalytic Cracking of N-Dodecane under Supercritical Conditions: In Situ SXAS and Xanes Studies. *ChemCatChem* **2017**, *9*, 99−102.
(31) Gilbert, J. A.; Kariuki, N. N.; Subbaraman, R.; Kropf, A. J.; Smith, M. C.; Holby, E. F.; Morgan, D.; Myers, D. J. In Situ Anomalous Small-Angle X-Ray Scattering Studies of Platinum Nanoparticle Fuel Cell Electrocatalyst Degradation. *J. Am. Chem. Soc.* **2012**, *134*, 14823−14833.
(32) Haubold, H. G.; Vad, T.; Waldofner, N.; Bonnemann, H. From Pt Molecules to Nanoparticles: In-Situ (Anomalous) Small-Angle X-Ray Scattering Studies. *J. Appl. Crystallogr.* **2003**, *36*, 617−620.
(33) Povia, M.; Herranz, J.; Binninger, T.; Nachtegaal, M.; Diaz, A.; Kohlbrecher, J.; Abbott, D. F.; Kim, B. J.; Schmidt, T. J. Combining SXAS and XAS to Study the Operando Degradation of Carbon-Supported Pt-Nanoparticle Fuel Cell Catalysts. *ACS Catal.* **2018**, *8*, 7000−7015.
(34) Tuaev, X.; Strasser, P. Small Angle X-Ray Scattering (SXAS) Techniques for Polymer Electrolyte Membrane Fuel Cell Characterization. *Woodhead Publ Ser. En* **2012**, 87−119.
(35) Ruge, M.; Drnec, J.; Rahn, B.; Reikowski, F.; Harrington, D. A.; Carlà, F.; Felici, R.; Stettner, J.; Magnussen, O. M. Structural Reorganization of Pt(111) Electrodes by Electrochemical Oxidation and Reduction. *J. Am. Chem. Soc.* **2017**, *139*, 4532−4539.
(36) Tuaev, X.; Rudi, S.; Petkov, V.; Hoell, A.; Strasser, P. In Situ Study of Atomic Structure Transformations of Pt-Ni Nanoparticle Catalysts During Electrochemical Potential Cycling. *ACS Nano* **2013**, *7*, 5666−5674.
(37) Roldan Cuenya, B. Metal Nanoparticle Catalysts Beginning to Shape-Up. *Acc. Chem. Res.* **2013**, *46*, 1682−1691.
(38) Matos, J.; Ono, L. K.; Behafarid, F.; Croy, J. R.; Mostafa, S.; DeLaRiva, A. T.; Datye, A. K.; Frenkel, A. I.; Roldan Cuenya, B. In Situ Coarsening Study of Inverse Micelle-Prepared Pt Nanoparticles Supported on Γ-Al_2O_3: Pretreatment and Environmental Effects. *Phys. Chem. Chem. Phys.* **2012**, *14*, 11457−11467.
(39) Grosse, P.; Gao, D.; Scholten, F.; Sinev, I.; Mistry, H.; Roldan Cuenya, B. Dynamic Changes in the Structure, Chemical State and Catalytic Selectivity of Cu Nanocubes During CO_2 Electroreduction: Size and Support Effects. *Angew. Chem., Int. Ed.* **2018**, *57*, 6192−6197.
(40) Deng, X.; Galli, F.; Koper, M. T. M. In Situ Electrochemical Afm Imaging of a Pt Electrode in Sulfuric Acid under Potential Cycling Conditions. *J. Am. Chem. Soc.* **2018**, *140*, 13285−13291.
(41) Ono, L. K.; Behafarid, F.; Cuenya, B. R. Nano-Gold Diggers: Au-Assisted SiO_2-Decomposition and Desorption in Supported Nanocatalysts. *ACS Nano* **2013**, *7*, 10327−10334.
(42) Martin, O.; Mondelli, C.; Cervellino, A.; Ferri, D.; Curulla-Ferre, D.; Perez-Ramirez, J. Operando Synchrotron X-Ray Powder Diffraction and Modulated-Excitation Infrared Spectroscopy Elucidate the CO_2 Promotion on a Commercial Methanol Synthesis Catalyst. *Angew. Chem., Int. Ed.* **2016**, *55*, 11031−6.
(43) Li, Y.; Zakharov, D.; Zhao, S.; Tappero, R.; Jung, U.; Elsen, A.; Baumann, P.; Nuzzo, R. G.; Stach, E. A.; Frenkel, A. I. Complex Structural Dynamics of Nanocatalysts Revealed in Operando Conditions by Correlated Imaging and Spectroscopy Probes. *Nat. Commun.* **2015**, *6*, 7583.
(44) Ganzler, A. M.; Casapu, M.; Vernoux, P.; Loridant, S.; Cadete Santos Aires, F. J.; Epicier, T.; Betz, B.; Hoyer, R.; Grunwaldt, J. D. Tuning the Structure of Platinum Particles on Ceria in Situ for Enhancing the Catalytic Performance of Exhaust Gas Catalysts. *Angew. Chem., Int. Ed.* **2017**, *56*, 13078−13082.
(45) Liang, Y.; Pfisterer, J. H. K.; McLaughlin, D.; Csoklich, C.; Seidl, L.; Bandarenka, A. S.; Schneider, O. Electrochemical Scanning Probe Microscopies in Electrocatalysis. *Small Methods* **2019**, *3*, 1800387.
(46) Beermann, V.; Holtz, M. E.; Padgett, E.; de Araujo, J. F.; Muller, D. A.; Strasser, P. Real-Time Imaging of Activation and Degradation of Carbon Supported Octahedral Pt−Ni Alloy Fuel Cell Catalysts at the Nanoscale Using in Situ Electrochemical Liquid Cell Stem. *Energy Environ. Sci.* **2019**, *12*, 2476.
(47) Yu, Y. C.; Xin, H. L. L.; Hovden, R.; Wang, D. L.; Rus, E. D.; Mundy, J. A.; Muller, D. A.; Abruna, H. D. Three-Dimensional Tracking and Visualization of Hundreds of Pt-Co Fuel Cell Nanocatalysts During Electrochemical Aging. *Nano Lett.* **2012**, *12*, 4417−4423.
(48) Schlogl, K.; Mayrhofer, K. J. J.; Hanzlik, M.; Arenz, M. Identical-Location Tem Investigations of Pt/C Electrocatalyst Degradation at Elevated Temperatures. *J. Electroanal. Chem.* **2011**, *662*, 355−360.
(49) Hengge, K.; Gansler, T.; Pizzutilo, E.; Heinzl, C.; Beetz, M.; Mayrhofer, K. J. J.; Scheu, C. Accelerated Fuel Cell Tests of Anodic Pt/Ru Catalyst Via Identical Location Tem: New Aspects of Degradation Behavior. *Int. J. Hydrogen Energy* **2017**, *42*, 25359−25371.
(50) Aran-Ais, R. M.; Yu, Y.; Hovden, R.; Solla-Gullon, J.; Herrero, E.; Feliu, J. M.; Abruna, H. D. Identical Location Transmission Electron Microscopy Imaging of Site-Selective Pt Nanocatalysts: Electrochemical Activation and Surface Disordering. *J. Am. Chem. Soc.* **2015**, *137*, 14992−8.
(51) Povia, M.; Herranz, J.; Binninger, T.; Nachtegaal, M.; Diaz, A.; Kohlbrecher, J.; Abbott, D. F.; Kim, B.-J.; Schmidt, T. J. Combining SXAS and XAS to Study the Operando Degradation of Carbon-Supported Pt-Nanoparticle Fuel Cell Catalysts. *ACS Catal.* **2018**, *8*, 7000−7015.
(52) Jacobse, L.; Huang, Y. F.; Koper, M. T. M.; Rost, M. J. Correlation of Surface Site Formation to Nanoisland Growth in the Electrochemical Roughening of Pt(111). *Nat. Mater.* **2018**, *17*, 277−282.
(53) Zhang, H.; Li, J.; Cheng, M.-J.; Lu, Q. Co Electroreduction: Current Development and Understanding of Cu-Based Catalysts. *ACS Catal.* **2019**, *9*, 49−65.
(54) Hori, Y.; Wakebe, H.; Tsukamoto, T.; Koga, O. Electrocatalytic Process of Co Selectivity in Electrochemical Reduction of CO_2 at Metal Electrodes in Aqueous Media. *Electrochim. Acta* **1994**, *39*, 1833−1839.
(55) Hori, Y.; Murata, A.; Takahashi, R. Formation of Hydrocarbons in the Electrochemical Reduction of Carbon Dioxide at a Copper Electrode in Aqueous Solution. *J. Chem. Soc., Faraday Trans. 1* **1989**, *85*, 2309−2326.
(56) Arán-Ais, R. M.; Gao, D.; Roldan Cuenya, B. Structure- and Electrolyte-Sensitivity in CO_2 Electroreduction. *Acc. Chem. Res.* **2018**, *51*, 2906−2917.
(57) Cao, S.; Tao, F. F.; Tang, Y.; Li, Y.; Yu, J. Size- and Shape-Dependent Catalytic Performances of Oxidation and Reduction Reactions on Nanocatalysts. *Chem. Soc. Rev.* **2016**, *45*, 4747−65.
(58) Wu, J.; Gross, A.; Yang, H. Shape and Composition-Controlled Platinum Alloy Nanocrystals Using Carbon Monoxide as Reducing Agent. *Nano Lett.* **2011**, *11*, 798−802.
(59) Bajdich, M.; Garcia-Mota, M.; Vojvodic, A.; Norskov, J. K.; Bell, A. T. Theoretical Investigation of the Activity of Cobalt Oxides for the Electrochemical Oxidation of Water. *J. Am. Chem. Soc.* **2013**, *135*, 13521−30.
(60) Solla-Gullon, J.; Vidal-Iglesias, F. J.; Feliu, J. M. Shape Dependent Electrocatalysis. *Annu. Rep. Prog. Chem., Sect. C: Phys. Chem.* **2011**, *107*, 263−297.
(61) Calle-Vallejo, F.; Martinez, J. I.; Garcia-Lastra, J. M.; Sautet, P.; Loffreda, D. Fast Prediction of Adsorption Properties for Platinum Nanocatalysts with Generalized Coordination Numbers. *Angew. Chem., Int. Ed.* **2014**, *53*, 8316−9.
(62) Calle-Vallejo, F.; Tymoczko, J.; Colic, V.; Vu, Q. H.; Pohl, M. D.; Morgenstern, K.; Loffreda, D.; Sautet, P.; Schuhmann, W.; Bandarenka, A. S. Finding Optimal Surface Sites on Heterogeneous Catalysts by Counting Nearest Neighbors. *Science* **2015**, *350*, 185.

DOI: 10.1021/acscatal.9b01831
ACS Catal. 2019, 9, 10020−10043

(63) Avanesian, T.; Dai, S.; Kale, M. J.; Graham, G. W.; Pan, X.; Christopher, P. Quantitative and Atomic-Scale View of CO-Induced Pt Nanoparticle Surface Reconstruction at Saturation Coverage Via Dft Calculations Coupled with *in Situ* TEM and IR. *J. Am. Chem. Soc.* **2017**, *139*, 4551−4558.
(64) Fujita, T.; Tokunaga, T.; Zhang, L.; Li, D.; Chen, L.; Arai, S.; Yamamoto, Y.; Hirata, A.; Tanaka, N.; Ding, Y.; Chen, M. Atomic Observation of Catalysis-Induced Nanopore Coarsening of Nanoporous Gold. *Nano Lett.* **2014**, *14*, 1172−7.
(65) Dai, S.; Hou, Y.; Onoue, M.; Zhang, S.; Gao, W.; Yan, X.; Graham, G. W.; Wu, R.; Pan, X. Revealing Surface Elemental Composition and Dynamic Processes Involved in Facet-Dependent Oxidation of Pt_3Co Nanoparticles Via in Situ Transmission Electron Microscopy. *Nano Lett.* **2017**, *17*, 4683−4688.
(66) Meng, J.; Zhu, B.; Gao, Y. Shape Evolution of Metal Nanoparticles in Binary Gas Environment. *J. Phys. Chem. C* **2018**, *122*, 6144−6150.
(67) Jorgensen, M.; Gronbeck, H. The Site-Assembly Determines Catalytic Activity of Nanoparticles. *Angew. Chem., Int. Ed.* **2018**, *57*, 5086−5089.
(68) Zugic, B.; Wang, L.; Heine, C.; Zakharov, D. N.; Lechner, B. A. J.; Stach, E. A.; Biener, J.; Salmeron, M.; Madix, R. J.; Friend, C. M. Dynamic Restructuring Drives Catalytic Activity on Nanoporous Gold-Silver Alloy Catalysts. *Nat. Mater.* **2017**, *16*, 558−564.
(69) Cabié, M.; Giorgio, S.; Henry, C. R.; Axet, M. R.; Philippot, K.; Chaudret, B. Direct Observation of the Reversible Changes of the Morphology of Pt Nanoparticles under Gas Environment. *J. Phys. Chem. C* **2010**, *114*, 2160−2163.
(70) Vendelbo, S. B.; Elkjær, C. F.; Falsig, H.; Puspitasari, I.; Dona, P.; Mele, L.; Morana, B.; Nelissen, B. J.; van Rijn, R.; Creemer, J. F.; Kooyman, P. J.; Helveg, S. Visualization of Oscillatory Behaviour of Pt Nanoparticles Catalysing CO Oxidation. *Nat. Mater.* **2014**, *13*, 884.
(71) Uchiyama, T.; Yoshida, H.; Kuwauchi, Y.; Ichikawa, S.; Shimada, S.; Haruta, M.; Takeda, S. Systematic Morphology Changes of Gold Nanoparticles Supported on CeO_2 During CO Oxidation. *Angew. Chem., Int. Ed.* **2011**, *50*, 10157−10160.
(72) He, Y.; Liu, J. C.; Luo, L.; Wang, Y. G.; Zhu, J.; Du, Y.; Li, J.; Mao, S. X.; Wang, C. Size-Dependent Dynamic Structures of Supported Gold Nanoparticles in CO Oxidation Reaction Condition. *Proc. Natl. Acad. Sci. U. S. A.* **2018**, *115*, 7700−7705.
(73) Zasada, F.; Piskorz, W.; Sojka, Z. Cobalt Spinel at Various Redox Conditions: Dft+U Investigations into the Structure and Surface Thermodynamics of the (100) Facet. *J. Phys. Chem. C* **2015**, *119*, 19180−19191.
(74) Rahm, J. M.; Erhart, P. Beyond Magic Numbers: Atomic Scale Equilibrium Nanoparticle Shapes for Any Size. *Nano Lett.* **2017**, *17*, 5775−5781.
(75) Zasada, F.; Piskorz, W.; Stelmachowski, P.; Kotarba, A.; Paul, J.-F.; Płociński, T.; Kurzydłowski, K. J.; Sojka, Z. Periodic Dft and Hr-Stem Studies of Surface Structure and Morphology of Cobalt Spinel Nanocrystals. Retrieving 3d Shapes from 2d Images. *J. Phys. Chem. C* **2011**, *115*, 6423−6432.
(76) García-Mota, M.; Rieger, M.; Reuter, K. Ab Initio Prediction of the Equilibrium Shape of Supported Ag Nanoparticles on α-Al_2O_3 (0 0 0 1). *J. Catal.* **2015**, *321*, 1−6.
(77) Cheula, R.; Soon, A.; Maestri, M. Prediction of Morphological Changes of Catalyst Materials under Reaction Conditions by Combined Ab Initio Thermodynamics and Microkinetic Modelling. *Catal. Sci. Technol.* **2018**, *8*, 3493−3503.
(78) Duan, M.; Yu, J.; Meng, J.; Zhu, B.; Wang, Y.; Gao, Y. Reconstruction of Supported Metal Nanoparticles in Reaction Conditions. *Angew. Chem., Int. Ed.* **2018**, *57*, 6464−6469.
(79) Hu, C. H.; Chizallet, C.; Mager-Maury, C.; Corral-Valero, M.; Sautet, P.; Toulhoat, H.; Raybaud, P. Modulation of Catalyst Particle Structure Upon Support Hydroxylation: Ab Initio Insights into Pd_{13} and Pt_{13}/γ-Al_2O_3. *J. Catal.* **2010**, *274*, 99−110.
(80) Zhu, B.; Meng, J.; Gao, Y. Equilibrium Shape of Metal Nanoparticles under Reactive Gas Conditions. *J. Phys. Chem. C* **2017**, *121*, 5629−5634.
(81) Zhu, B.; Xu, Z.; Wang, C.; Gao, Y. Shape Evolution of Metal Nanoparticles in Water Vapor Environment. *Nano Lett.* **2016**, *16*, 2628−32.
(82) Nolte, P.; Stierle, A.; Jin-Phillipp, N. Y.; Kasper, N.; Schulli, T. U.; Dosch, H. Shape Changes of Supported Rh Nanoparticles During Oxidation and Reduction Cycles. *Science* **2008**, *321*, 1654.
(83) Yan, Z.; Taylor, M. G.; Mascareno, A.; Mpourmpakis, G. Size-, Shape-, and Composition-Dependent Model for Metal Nanoparticle Stability Prediction. *Nano Lett.* **2018**, *18*, 2696−2704.
(84) Mistry, H.; Behafarid, F.; Bare, S. R.; Roldan Cuenya, B. Pressure-Dependent Effect of Hydrogen Adsorption on Structural and Electronic Properties of Pt/Gamma-Al_2O_3 Nanoparticles. *ChemCatChem* **2014**, *6*, 348−352.
(85) Matsubu, J. C.; Zhang, S.; DeRita, L.; Marinkovic, N. S.; Chen, J. G.; Graham, G. W.; Pan, X.; Christopher, P. Adsorbate-Mediated Strong Metal-Support Interactions in Oxide-Supported Rh Catalysts. *Nat. Chem.* **2017**, *9*, 120−127.
(86) Lunkenbein, T.; Schumann, J.; Behrens, M.; Schlögl, R.; Willinger, M. G. Formation of a Zno Overlayer in Industrial Cu/ZnO/Al_2O_3 Catalysts Induced by Strong Metal−Support Interactions. *Angew. Chem.* **2015**, *127*, 4627−4631.
(87) Xu, Y.; Getman, R. B.; Shelton, W. A.; Schneider, W. F. A First-Principles Investigation of the Effect of Pt Cluster Size on CO and NO Oxidation Intermediates and Energetics. *Phys. Chem. Chem. Phys.* **2008**, *10*, 6009−18.
(88) Mager-Maury, C.; Bonnard, G.; Chizallet, C.; Sautet, P.; Raybaud, P. H2-Induced Reconstruction of Supported Pt Clusters: Metal-Support Interaction Versus Surface Hydride. *ChemCatChem* **2011**, *3*, 200−207.
(89) Calle-Vallejo, F.; Pohl, M. D.; Reinisch, D.; Loffreda, D.; Sautet, P.; Bandarenka, A. S. Why Conclusions from Platinum Model Surfaces Do Not Necessarily Lead to Enhanced Nanoparticle Catalysts for the Oxygen Reduction Reaction. *Chem. Sci.* **2017**, *8*, 2283−2289.
(90) Liu, J. X.; Filot, I. A. W.; Su, Y.; Zijlstra, B.; Hensen, E. J. M. Optimum Particle Size for Gold-Catalyzed CO Oxidation. *J. Phys. Chem. C* **2018**, *122*, 8327−8340.
(91) Schneider, W. F.; Hass, K. C.; Ramprasad, R.; Adams, J. B. Cluster Models of Cu Binding and CO and NO Adsorption in Cu-Exchanged Zeolites. *J. Phys. Chem.* **1996**, *100*, 6032−6046.
(92) Xu, Y.; Shelton, W. A.; Schneider, W. F. Effect of Particle Size on the Oxidizability of Platinum Clusters. *J. Phys. Chem. A* **2006**, *110*, 5839−5846.
(93) Mierwaldt, D.; Roddatis, V.; Risch, M.; Scholz, J.; Geppert, J.; Abrishami, M. E.; Jooss, C. Environmental Tem Investigation of Electrochemical Stability of Perovskite and Ruddlesden-Popper Type Manganite Oxygen Evolution Catalysts. *Advanced Sustainable Systems* **2017**, *1*, 1700109.
(94) Zhang, D.; Jin, C.; Li, Z. Y.; Zhang, Z.; Li, J. Oxidation Behavior of Cobalt Nanoparticles Studied by in Situ Environmental Transmission Electron Microscopy. *Science Bulletin* **2017**, *62*, 775−778.
(95) Hung, L. I.; Tsung, C. K.; Huang, W.; Yang, P. Room-Temperature Formation of Hollow Cu(2)O Nanoparticles. *Adv. Mater.* **2010**, *22*, 1910−4.
(96) Nakamura, R.; Tokozakura, D.; Nakajima, H.; Lee, J. G.; Mori, H. Hollow Oxide Formation by Oxidation of Al and Cu Nanoparticles. *J. Appl. Phys.* **2007**, *101*, 074303.
(97) Tauster, S. J. Strong Metal-Support Interactions. *Acc. Chem. Res.* **1987**, *20*, 389−394.
(98) Zhang, S.; Plessow, P. N.; Willis, J. J.; Dai, S.; Xu, M.; Graham, G. W.; Cargnello, M.; Abild-Pedersen, F.; Pan, X. Dynamical Observation and Detailed Description of Catalysts under Strong Metal-Support Interaction. *Nano Lett.* **2016**, *16*, 4528−34.
(99) Ahmadi, M.; Timoshenko, J.; Behafarid, F.; Roldan Cuenya, B. Tuning the Structure of Pt Nanoparticles through Support Interactions: An in Situ Polarized X-Ray Absorption Study Coupled with Atomistic Simulations. *J. Phys. Chem. C* **2019**, *123*, 10666−10676.

DOI: 10.1021/acscatal.9b01831
ACS Catal. 2019, 9, 10020−10043

(100) Ahmadi, M.; Mistry, H.; Roldan Cuenya, B. Tailoring the Catalytic Properties of Metal Nanoparticles Via Support Interactions. *J. Phys. Chem. Lett.* **2016**, *7*, 3519−3533.
(101) Wu, H.; Fu, Q.; Li, Y.; Cui, Y.; Wang, R.; Su, N.; Lin, L.; Dong, A.; Ning, Y.; Yang, F.; Bao, X. Controlled Growth of Uniform Two-Dimensional ZnO Overlayers on Au(111) and Surface Hydroxylation. *Nano Res.* **2019**, *12*, 2348.
(102) Behrens, M.; Studt, F.; Kasatkin, I.; Kühl, S.; Hävecker, M.; Abild-Pedersen, F.; Zander, S.; Girgsdies, F.; Kurr, P.; Kniep, B.-L.; Tovar, M.; Fischer, R. W.; Nørskov, J. K.; Schlögl, R. The Active Site of Methanol Synthesis over $Cu/ZnO/Al_2O_3$ Industrial Catalysts. *Science* **2012**, *336*, 893−897.
(103) Kattel, S.; Ramírez, P. J.; Chen, J. G.; Rodriguez, J. A.; Liu, P. Active sites for CO_2 hydrogenation to methanol on Cu/ZnO catalysts. *Science* **2017**, *355*, 1296.
(104) Kandemir, T.; Girgsdies, F.; Hansen, T. C.; Liss, K.-D.; Kasatkin, I.; Kunkes, E. L.; Wowsnick, G.; Jacobsen, N.; Schlögl, R.; Behrens, M. In Situ Study of Catalytic Processes: Neutron Diffraction of a Methanol Synthesis Catalyst at Industrially Relevant Pressure. *Angew. Chem., Int. Ed.* **2013**, *52*, 5166−5170.
(105) Farmer, J. A.; Campbell, C. T. Ceria Maintains Smaller Metal Catalyst Particles by Strong Metal-Support Bonding. *Science* **2010**, *329*, 933.
(106) Behafarid, F.; Roldan Cuenya, B. Coarsening Phenomena of Metal Nanoparticles and the Influence of the Support Pre-Treatment: $Pt/TiO_2(110)$. *Surf. Sci.* **2012**, *606*, 908−918.
(107) Artero, V.; Fontecave, M. Solar Fuels Generation and Molecular Systems: Is It Homogeneous or Heterogeneous Catalysis? *Chem. Soc. Rev.* **2013**, *42*, 2338−2356.
(108) Li, J.; Guttinger, R.; More, R.; Song, F.; Wan, W.; Patzke, G. R. Frontiers of Water Oxidation: The Quest for True Catalysts. *Chem. Soc. Rev.* **2017**, *46*, 6124−6147.
(109) Stracke, J. J.; Finke, R. G. Distinguishing Homogeneous from Heterogeneous Water Oxidation Catalysis When Beginning with Polyoxometalates. *ACS Catal.* **2014**, *4*, 909−933.
(110) Lee, K. J.; McCarthy, B. D.; Dempsey, J. L. On Decomposition, Degradation, and Voltammetric Deviation: The Electrochemist's Field Guide to Identifying Precatalyst Transformation. *Chem. Soc. Rev.* **2019**, *48*, 2927−2945.
(111) Yin, Q. S.; Tan, J. M.; Besson, C.; Geletii, Y. V.; Musaev, D. G.; Kuznetsov, A. E.; Luo, Z.; Hardcastle, K. I.; Hill, C. L. A Fast Soluble Carbon-Free Molecular Water Oxidation Catalyst Based on Abundant Metals. *Science* **2010**, *328*, 342−345.
(112) Stracke, J. J.; Finke, R. G. Water Oxidation Catalysis Beginning with 2.5 Mm $[Co_4(H_2O)_2(Pw_9O_{34})_2]^{10-}$: Investigation of the True Electrochemically Driven Catalyst at ≥ 600 mV Overpotential at a Glassy Carbon Electrode. *ACS Catal.* **2013**, *3*, 1209−1219.
(113) Stracke, J. J.; Finke, R. G. Water Oxidation Catalysis Beginning with $Co_4(H_2O)_2(PW_9O_{34})_2^{10-}$ When Driven by the Chemical Oxidant Ruthenium(Iii)Tris(2,2′-Bipyridine): Stoichiometry, Kinetic, and Mechanistic Studies En Route to Identifying the True Catalyst. *ACS Catal.* **2014**, *4*, 79−89.
(114) Goberna-Ferrón, S.; Soriano-López, J.; Galán-Mascarós, J. R.; Nyman, M. Solution Speciation and Stability of Cobalt-Polyoxometalate Water Oxidation Catalysts by X-Ray Scattering. *Eur. J. Inorg. Chem.* **2015**, *2015*, 2833−2840.
(115) Goberna-Ferron, S.; Vigara, L.; Soriano-Lopez, J.; Galan-Mascaros, J. R. Identification of a Nonanuclear {Co(Ii)9} Polyoxometalate Cluster as a Homogeneous Catalyst for Water Oxidation. *Inorg. Chem.* **2012**, *51*, 11707−15.
(116) Stracke, J. J.; Finke, R. G. Electrocatalytic Water Oxidation Beginning with the Cobalt Polyoxometalate $[Co_4(H_2O)_2(PW_9O_{34})_2]^{10-}$: Identification of Heterogeneous Coox as the Dominant Catalyst. *J. Am. Chem. Soc.* **2011**, *133*, 14872−5.
(117) Anxolabehere-Mallart, E.; Costentin, C.; Fournier, M.; Nowak, S.; Robert, M.; Saveant, J. M. Boron-Capped Tris(Glyoximato) Cobalt Clathrochelate as a Precursor for the Electrodeposition of Nanoparticles Catalyzing H_2 Evolution in Water. *J. Am. Chem. Soc.* **2012**, *134*, 6104−7.
(118) Lassalle-Kaiser, B.; Zitolo, A.; Fonda, E.; Robert, M.; Anxolabéhère-Mallart, E. In Situ Observation of the Formation and Structure of Hydrogen-Evolving Amorphous Cobalt Electrocatalysts. *ACS Energy Letters* **2017**, *2*, 2545−2551.
(119) Coperet, C. Single-Sites and Nanoparticles at Tailored Interfaces Prepared Via Surface Organometallic Chemistry from Thermolytic Molecular Precursors. *Acc. Chem. Res.* **2019**, *52*, 1697−1708.
(120) Lam, E.; Larmier, K.; Wolf, P.; Tada, S.; Safonova, O. V.; Copéret, C. Isolated Zr Surface Sites on Silica Promote Hydrogenation of CO_2 to Ch_3OH in Supported Cu Catalysts. *J. Am. Chem. Soc.* **2018**, *140*, 10530−10535.
(121) Noh, G.; Lam, E.; Alfke, J. L.; Larmier, K.; Searles, K.; Wolf, P.; Copéret, C. Selective Hydrogenation of CO_2 to CH_3OH on Supported Cu Nanoparticles Promoted by Isolated Tiiv Surface Sites on SiO_2. *ChemSusChem* **2019**, *12*, 968−972.
(122) Searles, K.; Chan, K. W.; Mendes Burak, J. A.; Zemlyanov, D.; Safonova, O.; Copéret, C. Highly Productive Propane Dehydrogenation Catalyst Using Silica-Supported Ga−Pt Nanoparticles Generated from Single-Sites. *J. Am. Chem. Soc.* **2018**, *140*, 11674−11679.
(123) Binninger, T.; Fabbri, E.; Patru, A.; Garganourakis, M.; Han, J.; Abbott, D. F.; Sereda, O.; Kotz, R.; Menzel, A.; Nachtegaal, M.; Schmidt, T. J. Electrochemical Flow-Cell Setup for in Situ X-Ray Investigations I. Cell for SXAS and XAS at Synchrotron Facilities. *J. Electrochem. Soc.* **2016**, *163*, H906−H912.
(124) Friebel, D.; Miller, D. J.; O'Grady, C. P.; Anniyev, T.; Bargar, J.; Bergmann, U.; Ogasawara, H.; Wikfeldt, K. T.; Pettersson, L. G.; Nilsson, A. In Situ X-Ray Probing Reveals Fingerprints of Surface Platinum Oxide. *Phys. Chem. Chem. Phys.* **2011**, *13*, 262−6.
(125) Klingan, K.; Kottakkat, T.; Jovanov, Z. P.; Jiang, S.; Pasquini, C.; Scholten, F.; Kubella, P.; Bergmann, A.; Cuenya, B.; Roth, C.; Dau, H. Reactivity Determinants in Electrodeposited Cu Foams for Electrochemical CO_2 Reduction. *ChemSusChem* **2018**, *11*, 3449−3459.
(126) Merte, L. R.; Behafarid, F.; Miller, D. J.; Friebel, D.; Cho, S.; Mbuga, F.; Sokaras, D.; Alonso-Mori, R.; Weng, T.-C.; Nordlund, D.; Nilsson, A.; Roldan Cuenya, B. Electrochemical Oxidation of Size-Selected Pt Nanoparticles Studied Using in Situ High-Energy-Resolution X-Ray Absorption Spectroscopy. *ACS Catal.* **2012**, *2*, 2371−2376.
(127) Rodriguez, J. A.; Hanson, J. C.; Stacchiola, D.; Senanayake, S. D. In Situ/Operando Studies for the Production of Hydrogen through the Water-Gas Shift on Metal Oxide Catalysts. *Phys. Chem. Chem. Phys.* **2013**, *15*, 12004−25.
(128) Seo, B.; Sa, Y. J.; Woo, J.; Kwon, K.; Park, J.; Shin, T. J.; Jeong, H. Y.; Joo, S. H. Size-Dependent Activity Trends Combined with in Situ X-Ray Absorption Spectroscopy Reveal Insights into Cobalt Oxide/Carbon Nanotube-Catalyzed Bifunctional Oxygen Electrocatalysis. *ACS Catal.* **2016**, *6*, 4347−4355.
(129) Tillier, J.; Binninger, T.; Garganourakis, M.; Patru, A.; Fabbri, E.; Schmidt, T. J.; Sereda, O. Electrochemical Flow-Cell Setup for in Situ X-Ray Investigations Ii. Cell for SXAS on a Multi-Purpose Laboratory Diffractometer. *J. Electrochem. Soc.* **2016**, *163*, H913−H920.
(130) Totir, D.; Mo, Y.; Kim, S.; Antonio, M. R.; Scherson, D. A. In Situ Co K-Edge X-Ray Absorption Fine Structure of Cobalt Hydroxide Film Electrodes in Alkaline Solutions. *J. Electrochem. Soc.* **2000**, *147*, 4594−4594.
(131) Risch, M.; Ringleb, F.; Kohlhoff, M.; Bogdanoff, P.; Chernev, P.; Zaharieva, I.; Dau, H. Water Oxidation by Amorphous Cobalt-Based Oxides: In Situ Tracking of Redox Transitions and Mode of Catalysis. *Energy Environ. Sci.* **2015**, *8*, 661−674.
(132) Zhang, D.; Jin, C.; Tian, H.; Xiong, Y.; Zhang, H.; Qiao, P.; Fan, J.; Zhang, Z.; Li, Z. Y.; Li, J. An in Situ TEM Study of the Surface Oxidation of Palladium Nanocrystals Assisted by Electron Irradiation. *Nanoscale* **2017**, *9*, 6327−6333.

DOI: 10.1021/acscatal.9b01831
ACS Catal. 2019, 9, 10020−10043

(133) Sasaki, K.; Marinkovic, N.; Isaacs, H. S.; Adzic, R. R. Synchrotron-Based in Situ Characterization of Carbon-Supported Platinum and Platinum Monolayer Electrocatalysts. *ACS Catal.* **2016**, *6*, 69−76.
(134) Drnec, J.; Ruge, M.; Reikowski, F.; Rahn, B.; Carlà, F.; Felici, R.; Stettner, J.; Magnussen, O. M.; Harrington, D. A. Initial Stages of Pt(111) Electrooxidation: Dynamic and Structural Studies by Surface X-Ray Diffraction. *Electrochim. Acta* **2017**, *224*, 220−227.
(135) Simonsen, S. B.; Chorkendorff, I.; Dahl, S.; Skoglundh, M.; Helveg, S. Coarsening of Pd Nanoparticles in an Oxidizing Atmosphere Studied by in Situ TEM. *Surf. Sci.* **2016**, *648*, 278−283.
(136) Zhang, X.; Meng, J.; Zhu, B.; Yu, J.; Zou, S.; Zhang, Z.; Gao, Y.; Wang, Y. In Situ TEM Studies of the Shape Evolution of Pd Nanocrystals under Oxygen and Hydrogen Environments at Atmospheric Pressure. *Chem. Commun. (Cambridge, U. K.)* **2017**, *53*, 13213−13216.
(137) Hejral, U.; Vlad, A.; Nolte, P.; Stierle, A. In Situ Oxidation Study of Pt Nanoparticles on MgO(001). *J. Phys. Chem. C* **2013**, *117*, 19955−19966.
(138) Nolte, P.; Stierle, A.; Balmes, O.; Srot, V.; van Aken, P. A.; Jeurgens, L. P. H.; Dosch, H. Carbon Incorporation and Deactivation of MgO(001) Supported Pd Nanoparticles During CO Oxidation. *Catal. Today* **2009**, *145*, 243−250.
(139) Nolte, P.; Stierle, A.; Kasper, N.; Jin-Phillipp, N. Y.; Reichert, H.; Rühm, A.; Okasinski, J.; Dosch, H.; Schöder, S. Combinatorial High-Energy X-Ray Microbeam Study of the Size-Dependent Oxidation of Pd Nanoparticles on MgO(100). *Phys. Rev. B: Condens. Matter Mater. Phys.* **2008**, *77*, 115444.
(140) Croy, J. R.; Mostafa, S.; Liu, J.; Sohn, Y.; Heinrich, H.; Cuenya, B. R. Support Dependence of Meoh Decomposition over Size-Selected Pt Nanoparticles. *Catal. Lett.* **2007**, *119*, 209−216.
(141) Merte, L. R.; Ahmadi, M.; Behafarid, F.; Ono, L. K.; Lira, E.; Matos, J.; Li, L.; Yang, J. C.; Roldan Cuenya, B. Correlating Catalytic Methanol Oxidation with the Structure and Oxidation State of Size-Selected Pt Nanoparticles. *ACS Catal.* **2013**, *3*, 1460−1468.
(142) Paredis, K.; Ono, L. K.; Mostafa, S.; Li, L.; Zhang, Z.; Yang, J. C.; Barrio, L.; Frenkel, A. I.; Cuenya, B. R. Structure, Chemical Composition, and Reactivity Correlations During the in Situ Oxidation of 2-Propanol. *J. Am. Chem. Soc.* **2011**, *133*, 6728−35.
(143) Hejral, U.; Franz, D.; Volkov, S.; Francoual, S.; Strempfer, J.; Stierle, A. Identification of a Catalytically Highly Active Surface Phase for Co Oxidation over Ptrh Nanoparticles under Operando Reaction Conditions. *Phys. Rev. Lett.* **2018**, *120*, 126101.
(144) Behafarid, F.; Roldan Cuenya, B. Nanoepitaxy Using Micellar Nanoparticles. *Nano Lett.* **2011**, *11*, 5290−5296.
(145) Viswanathan, V.; Hansen, H. A.; Rossmeisl, J.; Nørskov, J. K. Universality in Oxygen Reduction Electrocatalysis on Metal Surfaces. *ACS Catal.* **2012**, *2*, 1654−1660.
(146) Cherevko, S.; Kulyk, N.; Mayrhofer, K. J. J. Durability of Platinum-Based Fuel Cell Electrocatalysts: Dissolution of Bulk and Nanoscale Platinum. *Nano Energy* **2016**, *29*, 275−298.
(147) Topalov, A. A.; Katsounaros, I.; Auinger, M.; Cherevko, S.; Meier, J. C.; Klemm, S. O.; Mayrhofer, K. J. Dissolution of Platinum: Limits for the Deployment of Electrochemical Energy Conversion? *Angew. Chem., Int. Ed.* **2012**, *51*, 12613−5.
(148) Nong, H. N.; Reier, T.; Oh, H. S.; Gliech, M.; Paciok, P.; Vu, T. H. T.; Teschner, D.; Heggen, M.; Petkov, V.; Schlogl, R.; Jones, T.; Strasser, P. A Unique Oxygen Ligand Environment Facilitates Water Oxidation in Hole-Doped $IrNiO_x$ Core-Shell Electrocatalysts. *Nature Catalysis* **2018**, *1*, 841−851.
(149) Minguzzi, A.; Lugaresi, O.; Achilli, E.; Locatelli, C.; Vertova, A.; Ghigna, P.; Rondinini, S. Observing the Oxidation State Turnover in Heterogeneous Iridium-Based Water Oxidation Catalysts. *Chemical Science* **2014**, *5*, 3591−3597.
(150) Pfeifer, V.; Jones, T. E.; Velasco Velez, J. J.; Arrigo, R.; Piccinin, S.; Havecker, M.; Knop-Gericke, A.; Schlogl, R. In Situ Observation of Reactive Oxygen Species Forming on Oxygen-Evolving Iridium Surfaces. *Chem. Sci.* **2017**, *8*, 2143−2149.
(151) Pfeifer, V.; Jones, T. E.; Wrabetz, S.; Massué, C.; Velasco Vélez, J. J.; Arrigo, R.; Scherzer, M.; Piccinin, S.; Hävecker, M.; Knop-Gericke, A.; Schlögl, R. Reactive Oxygen Species in Iridium-Based OER Catalysts. *Chem. Sci.* **2016**, *7*, 6791−6795.
(152) Abbott, D. F.; Lebedev, D.; Waltar, K.; Povia, M.; Nachtegaal, M.; Fabbri, E.; Copéret, C.; Schmidt, T. J. Iridium Oxide for the Oxygen Evolution Reaction: Correlation between Particle Size, Morphology, and the Surface Hydroxo Layer from Operando XAS. *Chem. Mater.* **2016**, *28*, 6591−6604.
(153) Dionigi, F.; Strasser, P. NiFe-based (Oxy)Hydroxide Catalysts for Oxygen Evolution Reaction in Non-Acidic Electrolytes. *Adv. Energy Mater.* **2016**, *6*, 1600621.
(154) Bergmann, A.; Martinez-Moreno, E.; Teschner, D.; Chernev, P.; Gliech, M.; de Araujo, J. F.; Reier, T.; Dau, H.; Strasser, P. Reversible Amorphization and the Catalytically Active State of Crystalline Co_3O_4 During Oxygen Evolution. *Nat. Commun.* **2015**, *6*, 8625.
(155) Bergmann, A.; Jones, T. E.; Martinez Moreno, E.; Teschner, D.; Chernev, P.; Gliech, M.; Reier, T.; Dau, H.; Strasser, P. Unified Structural Motifs of the Catalytically Active State of Co(Oxyhydr)-Oxides During the Electrochemical Oxygen Evolution Reaction. *Nature Catalysis* **2018**, *1*, 711−719.
(156) Risch, M.; Grimaud, A.; May, K. J.; Stoerzinger, K. A.; Chen, T. J.; Mansour, A. N.; Shao-Horn, Y. Structural Changes of Cobalt-Based Perovskites Upon Water Oxidation Investigated by Exafs. *J. Phys. Chem. C* **2013**, *117*, 8628−8635.
(157) Tung, C. W.; Hsu, Y. Y.; Shen, Y. P.; Zheng, Y.; Chan, T. S.; Sheu, H. S.; Cheng, Y. C.; Chen, H. M. Reversible Adapting Layer Produces Robust Single-Crystal Electrocatalyst for Oxygen Evolution. *Nat. Commun.* **2015**, *6*, 8106.
(158) Kanan, M. W.; Yano, J.; Surendranath, Y.; Dinca, M.; Yachandra, V. K.; Nocera, D. G. Structure and Valency of a Cobalt-Phosphate Water Oxidation Catalyst Determined by in Situ X-Ray Spectroscopy. *J. Am. Chem. Soc.* **2010**, *132*, 13692−13701.
(159) Han, B.; Stoerzinger, K. A.; Tileli, V.; Gamalski, A. D.; Stach, E. A.; Shao-Horn, Y. Nanoscale Structural Oscillations in Perovskite Oxides Induced by Oxygen Evolution. *Nat. Mater.* **2017**, *16*, 121−126.
(160) Favaro, M.; Yang, J.; Nappini, S.; Magnano, E.; Toma, F. M.; Crumlin, E. J.; Yano, J.; Sharp, I. D. Understanding the Oxygen Evolution Reaction Mechanism on CoO_x Using Operando Ambient-Pressure X-Ray Photoelectron Spectroscopy. *J. Am. Chem. Soc.* **2017**, *139*, 8960−8970.
(161) Kandemir, T.; Friedrich, M.; Parker, S. F.; Studt, F.; Lennon, D.; Schlogl, R.; Behrens, M. Different Routes to Methanol: Inelastic Neutron Scattering Spectroscopy of Adsorbates on Supported Copper Catalysts. *Phys. Chem. Chem. Phys.* **2016**, *18*, 17253−8.
(162) Kuhl, S.; Tarasov, A.; Zander, S.; Kasatkin, I.; Behrens, M. Cu-Based Catalyst Resulting from a Cu,Zn,Al Hydrotalcite-Like Compound: A Microstructural, Thermoanalytical, and in Situ XAS Study. *Chem. - Eur. J.* **2014**, *20*, 3782−92.
(163) Liu, B.; van Schooneveld, M. M.; Cui, Y. T.; Miyawaki, J.; Harada, Y.; Eschemann, T. O.; de Jong, K. P.; Delgado-Jaime, M. U.; de Groot, F. M. F. In-Situ 2p3d Resonant Inelastic X-Ray Scattering Tracking Cobalt Nanoparticle Reduction. *J. Phys. Chem. C* **2017**, *121*, 17450−17456.
(164) Rochet, A.; Moizan, V.; Pichon, C.; Diehl, F.; Berliet, A.; Briois, V. In Situ and Operando Structural Characterisation of a Fischer−Tropsch Supported Cobalt Catalyst. *Catal. Today* **2011**, *171*, 186−191.
(165) Tsakoumis, N. E.; Voronov, A.; Rønning, M.; Beek, W. v.; Borg, Ø.; Rytter, E.; Holmen, A. Fischer−Tropsch Synthesis: An XAS/XRPD Combined in Situ Study from Catalyst Activation to Deactivation. *J. Catal.* **2012**, *291*, 138−148.
(166) du Plessis, H. E.; Forbes, R. P.; Barnard, W.; Erasmus, W. J.; Steuwer, A. In Situ Reduction Study of Cobalt Model Fischer−Tropsch Synthesis Catalysts. *Phys. Chem. Chem. Phys.* **2013**, *15*, 11640−5.

DOI: 10.1021/acscatal.9b01831
ACS Catal. 2019, 9, 10020−10043

(167) Nayak, C.; Jain, P.; Vinod, C. P.; Jha, S. N.; Bhattacharyya, D. Operando X-Ray Absorption Spectroscopy Study of the Fischer−Tropsch Reaction with a Co Catalyst. *J. Synchrotron Radiat.* **2019**, *26*, 137−144.
(168) Cats, K. H.; Weckhuysen, B. M. Combined Operando X-Ray Diffraction/Raman Spectroscopy of Catalytic Solids in the Laboratory: The Co/TiO_2 Fischer−Tropsch Synthesis Catalyst Showcase. *ChemCatChem* **2016**, *8*, 1531−1542.
(169) Dehghan, R.; Hansen, T. W.; Wagner, J. B.; Holmen, A.; Rytter, E.; Borg, Ø.; Walmsley, J. C. In-Situ Reduction of Promoted Cobalt Oxide Supported on Alumina by Environmental Transmission Electron Microscopy. *Catal. Lett.* **2011**, *141*, 754−761.
(170) Morales, F.; de Groot, F. M. F.; Glatzel, P.; Kleimenov, E.; Bluhm, H.; Hävecker, M.; Knop-Gericke, A.; Weckhuysen, B. M. In Situ X-Ray Absorption of Co/Mn/TiO_2catalysts for Fischer−Tropsch Synthesis. *J. Phys. Chem. B* **2004**, *108*, 16201−16207.
(171) Karaca, H.; Safonova, O. V.; Chambrey, S.; Fongarland, P.; Roussel, P.; Griboval-Constant, A.; Lacroix, M.; Khodakov, A. Y. Structure and Catalytic Performance of Pt-Promoted Alumina-Supported Cobalt Catalysts under Realistic Conditions of Fischer−Tropsch Synthesis. *J. Catal.* **2011**, *277*, 14−26.
(172) Rønning, M.; Tsakoumis, N. E.; Voronov, A.; Johnsen, R. E.; Norby, P.; van Beek, W.; Borg, Ø.; Rytter, E.; Holmen, A. Combined XRD and XANES Studies of a Re-Promoted Co/Γ-Al_2O_3 Catalyst at Fischer−Tropsch Synthesis Conditions. *Catal. Today* **2010**, *155*, 289−295.
(173) Tsakoumis, N. E.; Dehghan, R.; Johnsen, R. E.; Voronov, A.; van Beek, W.; Walmsley, J. C.; Borg, Ø.; Rytter, E.; Chen, D.; Rønning, M.; Holmen, A. A Combined in Situ XAS-XRPD-Raman Study of Fischer−Tropsch Synthesis over a Carbon Supported Co Catalyst. *Catal. Today* **2013**, *205*, 86−93.
(174) de Smit, E.; Beale, A. M.; Nikitenko, S.; Weckhuysen, B. M. Local and Long Range Order in Promoted Iron-Based Fischer−Tropsch Catalysts: A Combined in Situ X-Ray Absorption Spectroscopy/Wide Angle X-Ray Scattering Study. *J. Catal.* **2009**, *262*, 244−256.
(175) Jacobs, G.; Ji, Y.; Davis, B. H.; Cronauer, D.; Kropf, A. J.; Marshall, C. L. Fischer−Tropsch Synthesis: Temperature Programmed EXAFS/XANES Investigation of the Influence of Support Type, Cobalt Loading, and Noble Metal Promoter Addition to the Reduction Behavior of Cobalt Oxide Particles. *Appl. Catal., A* **2007**, *333*, 177−191.
(176) Melaet, G.; Ralston, W. T.; Li, C. S.; Alayoglu, S.; An, K.; Musselwhite, N.; Kalkan, B.; Somorjai, G. A. Evidence of Highly Active Cobalt Oxide Catalyst for the Fischer−Tropsch Synthesis and CO_2 Hydrogenation. *J. Am. Chem. Soc.* **2014**, *136*, 2260−3.
(177) LaGrow, A. P.; Ward, M. R.; Lloyd, D. C.; Gai, P. L.; Boyes, E. D. Visualizing the Cu/Cu2(O) Interface Transition in Nanoparticles with Environmental Scanning Transmission Electron Microscopy. *J. Am. Chem. Soc.* **2017**, *139*, 179−185.
(178) Zou, L.; Li, J.; Zakharov, D.; Stach, E. A.; Zhou, G. In Situ Atomic-Scale Imaging of the Metal/Oxide Interfacial Transformation. *Nat. Commun.* **2017**, *8*, 307.
(179) Cavalca, F.; Laursen, A. B.; Wagner, J. B.; Damsgaard, C. D.; Chorkendorff, I.; Hansen, T. W. Light-Induced Reduction of Cuprous Oxide in an Environmental Transmission Electron Microscope. *ChemCatChem* **2013**, *5*, 2667−2672.
(180) Sun, X.-P.; Sun, F.-F.; Gu, S.-Q.; Chen, J.; Du, X.-L.; Wang, J.-Q.; Huang, Y.-Y.; Jiang, Z. Local Structural Evolutions of Cuo/Zno/Al_2O_3 Catalyst for Methanol Synthesis under Operando Conditions Studied by in Situ Quick X-Ray Absorption Spectroscopy. *Nucl. Sci. Tech.* **2017**, *28*, 21.
(181) Kleymenov, E.; Sa, J.; Abu-Dahrieh, J.; Rooney, D.; van Bokhoven, J. A.; Troussard, E.; Szlachetko, J.; Safonova, O. V.; Nachtegaal, M. Structure of the Methanol Synthesis Catalyst Determined by *in Situ* HERFD-XAS and EXAFS. *Catal. Sci. Technol.* **2012**, *2*, 373−378.
(182) Yang, B.; Liu, C.; Halder, A.; Tyo, E. C.; Martinson, A. B. F.; Seifert, S.; Zapol, P.; Curtiss, L. A.; Vajda, S. Copper Cluster Size Effect in Methanol Synthesis from CO_2. *J. Phys. Chem. C* **2017**, *121*, 10406−10412.
(183) Beaumont, S. K. Recent Developments in the Application of Nanomaterials to Understanding Molecular Level Processes in Cobalt Catalysed Fischer−Tropsch Synthesis. *Phys. Chem. Chem. Phys.* **2014**, *16*, 5034−43.
(184) Xu, K.; Sun, B.; Lin, J.; Wen, W.; Pei, Y.; Yan, S.; Qiao, M.; Zhang, X.; Zong, B. Epsilon-Iron Carbide as a Low-Temperature Fischer−Tropsch Synthesis Catalyst. *Nat. Commun.* **2014**, *5*, 5783.
(185) Garza, A. J.; Bell, A. T.; Head-Gordon, M. Is Subsurface Oxygen Necessary for the Electrochemical Reduction of CO_2 on Copper? *J. Phys. Chem. Lett.* **2018**, *9*, 601−606.
(186) Ren, D.; Deng, Y. L.; Handoko, A. D.; Chen, C. S.; Malkhandi, S.; Yeo, B. S. Selective Electrochemical Reduction of Carbon Dioxide to Ethylene and Ethanol on Copper(I) Oxide Catalysts. *ACS Catal.* **2015**, *5*, 2814−2821.
(187) Ren, D.; Ang, B. S. H.; Yeo, B. S. Tuning the Selectivity of Carbon Dioxide Electroreduction toward Ethanol on Oxide-Derived Cuxzn Catalysts. *ACS Catal.* **2016**, *6*, 8239−8247.
(188) Deng, Y. L.; Yeo, B. S. Characterization of Electrocatalytic Water Splitting and CO_2 Reduction Reactions Using in Situ/Operando Raman Spectroscopy. *Ac. ACS Catal.* **2017**, *7*, 7873−7889.
(189) Dutta, A.; Kuzume, A.; Rahaman, M.; Vesztergom, S.; Broekmann, P. Monitoring the Chemical State of Catalysts for CO_2 Electroreduction: An in Operando Study. *ACS Catal.* **2015**, *5*, 7498−7502.
(190) Bañares, M. A.; Wachs, I. E. Molecular Structures of Supported Metal Oxide Catalysts under Different Environments. *J. Raman Spectrosc.* **2002**, *33*, 359−380.
(191) Eilert, A.; Cavalca, F.; Roberts, F. S.; Osterwalder, J.; Liu, C.; Favaro, M.; Crumlin, E. J.; Ogasawara, H.; Friebel, D.; Pettersson, L. G. M.; Nilsson, A. Subsurface Oxygen in Oxide-Derived Copper Electrocatalysts for Carbon Dioxide Reduction. *J. Phys. Chem. Lett.* **2017**, *8*, 285−290.
(192) Velasco-Vélez, J.-J.; Jones, T.; Gao, D.; Carbonio, E.; Arrigo, R.; Hsu, C.-J.; Huang, Y.-C.; Dong, C.-L.; Chen, J.-M.; Lee, J.-F.; Strasser, P.; Roldan Cuenya, B.; Schlögl, R.; Knop-Gericke, A.; Chuang, C.-H. The Role of the Copper Oxidation State in the Electrocatalytic Reduction of CO_2 into Valuable Hydrocarbons. *ACS Sustainable Chem. Eng.* **2019**, *7*, 1485−1492.
(193) De Luna, P.; Quintero-Bermudez, R.; Dinh, C.-T.; Ross, M. B.; Bushuyev, O. S.; Todorović, P.; Regier, T.; Kelley, S. O.; Yang, P.; Sargent, E. H. Catalyst Electro-Redeposition Controls Morphology and Oxidation State for Selective Carbon Dioxide Reduction. *Nature Catalysis* **2018**, *1*, 103−110.
(194) Eilert, A.; Roberts, F. S.; Friebel, D.; Nilsson, A. Formation of Copper Catalysts for CO_2 Reduction with High Ethylene/Methane Product Ratio Investigated with in Situ X-Ray Absorption Spectroscopy. *J. Phys. Chem. Lett.* **2016**, *7*, 1466−70.
(195) Mistry, H.; Varela, A. S.; Bonifacio, C. S.; Zegkinoglou, I.; Sinev, I.; Choi, Y. W.; Kisslinger, K.; Stach, E. A.; Yang, J. C.; Strasser, P.; Cuenya, B. R. Highly Selective Plasma-Activated Copper Catalysts for Carbon Dioxide Reduction to Ethylene. *Nat. Commun.* **2016**, *7*, 12123.
(196) Gao, D.; Zegkinoglou, I.; Divins, N. J.; Scholten, F.; Sinev, I.; Grosse, P.; Roldan Cuenya, B. Plasma-Activated Copper Nanocube Catalysts for Efficient Carbon Dioxide Electroreduction to Hydrocarbons and Alcohols. *ACS Nano* **2017**, *11*, 4825−4831.
(197) Kühl, S.; Strasser, P. Oxygen Electrocatalysis on Dealloyed Pt Nanocatalysts. *Top. Catal.* **2016**, *59*, 1628−1637.
(198) Gawande, M. B.; Goswami, A.; Asefa, T.; Guo, H.; Biradar, A. V.; Peng, D.-L.; Zboril, R.; Varma, R. S. Core−Shell Nanoparticles: Synthesis and Applications in Catalysis and Electrocatalysis. *Chem. Soc. Rev.* **2015**, *44*, 7540−7590.
(199) Liu, H.-l.; Nosheen, F.; Wang, X. Noble Metal Alloy Complex Nanostructures: Controllable Synthesis and Their Electrochemical Property. *Chem. Soc. Rev.* **2015**, *44*, 3056−3078.
(200) Wu, J.; Yang, H. Platinum-Based Oxygen Reduction Electrocatalysts. *Acc. Chem. Res.* **2013**, *46*, 1848−1857.

DOI: 10.1021/acscatal.9b01831
ACS Catal. 2019, 9, 10020−10043

(201) Guo, S.; Zhang, S.; Sun, S. Tuning Nanoparticle Catalysis for the Oxygen Reduction Reaction. *Angew. Chem., Int. Ed.* **2013**, *52*, 8526−8544.
(202) Escudero-Escribano, M.; Malacrida, P.; Hansen, M. H.; Vej-Hansen, U. G.; Velázquez-Palenzuela, A.; Tripkovic, V.; Schiøtz, J.; Rossmeisl, J.; Stephens, I. E. L.; Chorkendorff, I. Tuning the Activity of Pt Alloy Electrocatalysts by Means of the Lanthanide Contraction. *Science* **2016**, *352*, 73.
(203) Strasser, P.; Kuhl, S. Dealloyed Pt-Based Core-Shell Oxygen Reduction Electrocatalysts. *Nano Energy* **2016**, *29*, 166−177.
(204) Brodsky, C. N.; Young, A. P.; Ng, K. C.; Kuo, C. H.; Tsung, C. K. Electrochemically Induced Surface Metal Migration in Well-Defined Core-Shell Nanoparticles and Its General Influence on Electrocatalytic Reactions. *ACS Nano* **2014**, *8*, 9368−9378.
(205) Wellendorff, J.; Silbaugh, T. L.; Garcia-Pintos, D.; Nørskov, J. K.; Bligaard, T.; Studt, F.; Campbell, C. T. A Benchmark Database for Adsorption Bond Energies to Transition Metal Surfaces and Comparison to Selected DFT Functionals. *Surf. Sci.* **2015**, *640*, 36−44.
(206) Cui, C. H.; Gan, L.; Heggen, M.; Rudi, S.; Strasser, P. Compositional Segregation in Shaped Pt Alloy Nanoparticles and Their Structural Behaviour During Electrocatalysis. *Nat. Mater.* **2013**, *12*, 765−771.
(207) Tuaev, X.; Rudi, S.; Petkov, V.; Hoell, A.; Strasser, P. In Situ Study of Atomic Structure Transformations of Pt−Ni Nanoparticle Catalysts During Electrochemical Potential Cycling. *ACS Nano* **2013**, *7*, 5666−5674.
(208) Ahmadi, M.; Behafarid, F.; Cui, C. H.; Strasser, P.; Roldan Cuenya, B. Long-Range Segregation Phenomena in Shape-Selected Bimetallic Nanoparticles: Chemical State Effects. *ACS Nano* **2013**, *7*, 9195−9204.
(209) van Spronsen, M. A.; Daunmu, K.; O'Connor, C. R.; Egle, T.; Kersell, H.; Oliver-Meseguer, J.; Salmeron, M. B.; Madix, R. J.; Sautet, P.; Friend, C. M. Dynamics of Surface Alloys: Rearrangement of Pd/Ag(111) Induced by CO and O_2. *J. Phys. Chem. C* **2019**, *123*, 8312−8323.
(210) Pielsticker, L.; Zegkinoglou, I.; Divins, N. J.; Mistry, H.; Chen, Y. T.; Kostka, A.; Boscoboinik, J. A.; Cuenya, B. R. Segregation Phenomena in Size-Selected Bimetallic CuNi Nanoparticle Catalysts. *J. Phys. Chem. B* **2018**, *122*, 919−926.
(211) Kim, H. Y.; Henkelman, G. Co Adsorption-Driven Surface Segregation of Pd on Au/Pd Bimetallic Surfaces: Role of Defects and Effect on Co Oxidation. *ACS Catal.* **2013**, *3*, 2541−2546.
(212) Vignola, E.; Steinmann, S. N.; Vandegehuchte, B. D.; Curulla, D.; Sautet, P. C2h2-Induced Surface Restructuring of Pd−Ag Catalysts: Insights from Theoretical Modeling. *J. Phys. Chem. C* **2016**, *120*, 26320−26327.
(213) Zegkinoglou, I.; Pielsticker, L.; Han, Z. K.; Divins, N. J.; Kordus, D.; Chen, Y. T.; Escudero, C.; Perez-Dieste, V.; Zhu, B.; Gao, Y.; Cuenya, B. R. Surface Segregation in CuNi Nanoparticle Catalysts During CO_2 Hydrogenation: The Role of CO in the Reactant Mixture. *J. Phys. Chem. C* **2019**, *123*, 8421−8428.
(214) Reier, T.; Pawolek, Z.; Cherevko, S.; Bruns, M.; Jones, T.; Teschner, D.; Selve, S.; Bergmann, A.; Nong, H. N.; Schlögl, R.; Mayrhofer, K. J. J.; Strasser, P. Molecular Insight in Structure and Activity of Highly Efficient, Low-Ir Ir−Ni Oxide Catalysts for Electrochemical Water Splitting (OER). *J. Am. Chem. Soc.* **2015**, *137*, 13031−13040.
(215) Jahrman, E. P.; Holden, W. M.; Ditter, A. S.; Mortensen, D. R.; Seidler, G. T.; Fister, T. T.; Kozimor, S. A.; Piper, L. F. J.; Rana, J.; Hyatt, N. C.; Stennett, M. C. An Improved Laboratory-Based X-Ray Absorption Fine Structure and X-Ray Emission Spectrometer for Analytical Applications in Materials Chemistry Research. *Rev. Sci. Instrum.* **2019**, *90*, 024106.
(216) Malzer, W.; Grötzsch, D.; Gnewkow, R.; Schlesiger, C.; Kowalewski, F.; Van Kuiken, B.; DeBeer, S.; Kanngießer, B. A Laboratory Spectrometer for High Throughput X-Ray Emission Spectroscopy in Catalysis Research. *Rev. Sci. Instrum.* **2018**, *89*, 113111.
(217) Herlihy, D. M.; Waegele, M. M.; Chen, X.; Pemmaraju, C. D.; Prendergast, D.; Cuk, T. Detecting the Oxyl Radical of Photocatalytic Water Oxidation at an n-$SrTiO_3$/Aqueous Interface through Its Subsurface Vibration. *Nat. Chem.* **2016**, *8*, 549.
(218) Zhang, M.; Respinis, M. d.; Frei, H. Time-Resolved Observations of Water Oxidation Intermediates on a Cobalt Oxide Nanoparticle Catalyst. *Nat. Chem.* **2014**, *6*, 362−367.
(219) Öström, H.; Öberg, H.; Xin, H.; LaRue, J.; Beye, M.; Dell'Angela, M.; Gladh, J.; Ng, M. L.; Sellberg, J. A.; Kaya, S.; Mercurio, G.; Nordlund, D.; Hantschmann, M.; Hieke, F.; Kühn, D.; Schlotter, W. F.; Dakovski, G. L.; Turner, J. J.; Minitti, M. P.; Mitra, A.; Moeller, S. P.; Föhlisch, A.; Wolf, M.; Wurth, W.; Persson, M.; Nørskov, J. K.; Abild-Pedersen, F.; Ogasawara, H.; Pettersson, L. G. M.; Nilsson, A. Probing the Transition State Region in Catalytic CO Oxidation on Ru. *Science* **2015**, *347*, 978−982.

DOI: 10.1021/acscatal.9b01831
ACS Catal. 2019, 9, 10020−10043